Model Development and Monte Carlo Methods for the Simulation and Analysis of Coastal Impacts of Barrier Island Breach During Hurricanes

Catherine R. Jeffries

Dissertation submitted to the Faculty of the

Virginia Polytechnic Institute and State University

in partial fulfillment of the requirements for the degree of

Doctor of Philosophy

in

Geosciences

Robert Weiss, Chair

Jennifer Irish

Tina Dura

Tim Warburton

Justin Krometis

April 22, 2024

Blacksburg, Virginia

Keywords: Barrier Island breaching, storm surge modeling, model development, coastal hazards, Monte Carlo simulations

Model Development and Monte Carlo Methods for the Simulation and Analysis of Coastal Impacts of Barrier Island Breach During Hurricanes

Catherine R. Jeffries

(ABSTRACT)

Barrier islands can protect the mainland from flooding during storms through reduction of storm surge and dissipation of storm generated wave energy. However, the protective capability is reduced when barrier islands breach and a direct hydrodynamic connection between the water bodies on both sides of the barrier island is established. Breaching of barrier islands during large storm events is complicated, involving nonlinear processes that connect water, sediment transport, dune height, and island width among other factors. In order to assess the impacts barrier island breaching has on flooding on the mainland, we modified a storm surge model, GeoClaw, to impose a Gaussian bell-curve on the barrier island that opens during a hurricane simulation and deepened over time. We added a new method of generating storm surge with storm forcing inputs in the form of wind and pressure fields to expand GeoClaw's current utilization of best track information so that storm forcing from planetary boundary layer models can also be utilized in simulations. We created a statistical method to asses the sensitivity of mainland storm-surge to barrier island breaching by randomizing the location, time, and extent of a breach event across the barrier island at Moriches, NY. My results show that total mainland inundation is affected by the changes in location, size, timing and numbers of breaches. Total inundation has a logarithmic relationship with total breach area and breach location is an important predictor of inundation and bay surge. The insights from this study can help prepare shoreline communities for the

differing ways that breaching affects the mainland coastline. The model updates created can also allow others to use this framework to study differing regions. Understanding which mainland locations are vulnerable to breaching, planners and coastal engineers can design interventions to reduce the likelihood of a breach occurring in areas adjacent to high flood risk.

Model Development and Monte Carlo Methods for the Simulation and Analysis of Coastal Impacts of Barrier Island Breach During Hurricanes

Catherine R. Jeffries

(GENERAL AUDIENCE ABSTRACT)

Storm surge is one of the most deadly and expensive parts of a hurricane. Storm surge can be reduced if a barrier island exists near the mainland coastline. The sand dunes, beach vegetation, and size of the island aid in reducing the waves and storm-surge generated by large storms. When a barrier island breaches it causes a channel of water that connects the ocean and the bay that separates the island from the mainland. This channel of water allows waves and storm surge to be directly pushed into the bay, increasing the storm surge along the mainland coast. Breaching is complex with many factors such as dune size and total island width determining when or where a breach will form. In order to study how breaching affects the mainland during a hurricane, we chose a program that simulates storm surge from a hurricane, made a simple breaching calculation that opens a hole in a sand dune on a barrier island so that the ocean and bay are directly connected and the storm surge can pass through this hole, and enabled the program to use storm data that is pre-computed rather than generated during the simulation. In order to understand how breaching impacts the mainland coast at Moriches, NY, we simulated a hurricane and varied the number, size, and time of different breaches. We learned that total of all breach dimensions has a linear relationship to the amount of coastal flooding up to a threshold, where the breaches cover most of the island. Coastal communities can use the results of this study to determine where to put interventions in place that will reduce the impacts of barrier island breaching,

update flood risk maps, and warn community members of changes in their location's risk assessment. Additionally, other regions with barrier islands nearby can use the software updates we created to study their own regions and assess different risk patterns than this study.

Dedication

This dissertation is dedicated to my family and friends who spent countless hours lifting me up and encouraging to reach for my dreams and helping me along the way.

Acknowledgments

I would like to acknowledge and extend my thanks to my PhD supervisor Dr. Robert Weiss. Thank you for believing in me and your support over the course of this project.

To my parents, your love and unconditional support has been the main constant in my life and I could not have done this without you.

To my closest family, your willingness to always listen, offer feedback, and provide distraction when needed has been instrumental in my completion of this PhD.

Lastly, to my friends, your assistance with coding, guidance in how best to accomplish tasks I've set out to do and game nights to lighten the load have all kept me sane, thank you.

Contents

List of Figures

List of Tables

List of Abbreviations

ADCIRC Advanced Circulation Model

AMR Adaptive Mesh Refinement

SLOSH Sea Lake and Overland Surges from Hurricanes

SPLASH Special Program to List Amplitudes of Surges from Hurricanes

TC Tropical Cyclones

Chapter 1

Introduction

Tropical cyclones (TC) are one of the deadliest and costliest natural hazards modern society faces today [5]. Approximately 10% of the world's population lives in the low elevation coastal zone, defined as a coastal area that has an elevation under ten meters [43, 47]. One third of this global coastal population live in the 100-year flood plain, which puts them at higher risk of flooding induced by large storms such as hurricanes, nor'easters, and typhoons [47]. In the United States, Hurricane Katrina was the costliest TC in recorded history, with estimated damages at 108 billion dollars [5]. The Galveston hurricane of 1900 is considered the deadliest hurricane on record with an estimated 8000 deaths [5].

Tropical cyclones present many hazards to coastal communities; strong winds, increased rainfall, destructive wave activity, and storm surge can all significantly alter the environment near the coastline, causing damage to ecosystems and structures. One of the most destructive hazards generated by TCs is storm surge, an abnormal rise in sea level in response to wind and pressure forcing within the TC structure [46]. Storm surge of sufficient height will frequently overtop barriers, dunes, and other coastal infrastructure and inundate the mainland, leading to extensive flooding. During Hurricane Katrina, storm surge led to vast flooding along the Louisiana coast, which wrought much of the destruction.

In some places around the world and in the United States natural protective structures, called barrier islands, exist that help in mitigating the risks that tropical cyclones pose to coastlines. Barrier islands are long, shore-parallel, low-relief land masses that are adjacent to approximately 6.5% of the world's coastlines [48, 59]. Oertel [48] defines barrier island systems as containing six sedimentary environments: proximity to the mainland, a back-barrier region (bay or lagoon), an inlet and inlet delta, the barrier island, the barrier platform, and the shoreface. Barrier islands are protective structures that assist with dissipating the wave energy and storm surge approaching the mainland from the ocean. Barrier island dunes that are higher than the approaching storm surge cause wave breaking, which reduces the impact of the surge when it reaches the back-barrier bay [27, 48]. Low-lying dunes that are vegetated are more resistant to erosion and will absorb some of the seaward driven surge and wave energy.

Storm surge can be particularly devastating to barrier islands, causing inundation, erosion, and breaching. Breaching is defined as an opening in a narrow landmass that creates a direct hydrodynamic connection between the two adjacent bodies of water [33, 67]. Breaching of barrier islands during storms is a result of a complicated process of wave action, storm surge, overwash and the dimensions of the barrier island. Storm forcing combined with local bathymetry can create breaches in some areas, but not in others. Storm surge that causes a water level gradient between the ocean and back-barrier region will force water to flow rapidly over the barrier island and erode the sediment of the island in an effort to equalize the water level. This gradient involves a critical elevation of water levels that may not necessarily involve inundation of the island, but can still cause erosion [33, 37]. Storm surge and wave setup both increase the elevation of the water in the ocean and the back-barrier region; these water levels in addition to wave action reduce the stability of the barrier island dune slope [33, 37]. However, wave attack by itself, while weakening the dune slope, is unlikely to induce breaching because the net erosion is seaward and does not push erosion landward [50]. Breaching can occur through two different transport methods, overtopping (overwash) and seepage and liquefaction [33, 37].

During storm-induced overwash and inundation of the islands, the water flowing across the island can scour a channel between the sea and the back-barrier region [33, 50, 51]. For this scouring to occur, a strong flow and some duration of inundation are required. Breaching can occur from both the seaward and landward side of the barrier island, but field data is limited in its ability to illustrate from which direction a breach is initiated [33, 50, 58]. However, Smallegan and Irish [58] show that bay surge that comes after peak ocean surge is more likely to lead to breaching from the landward side of the barrier island. This is due to peak ocean surge having already weakened the dune through erosion caused by wave attack and swash [33, 58]. Breach location is challenging to correctly identify; localized lows in dune height and narrower portions of the barrier island are more likely to be potential breach locations [33, 35]. One study by van der Lugt et al. [62] simulated Hurricane Sandy (2012), combining boundary conditions of surge-tide levels, 2D wave-spectra, and sediment transport to illustrate barrier island morphodynamics during the hurricane using pre-storm LiDAR generated bathymetric grids. This simulation employed a sediment transport model which generated two breaches at locations where the model calculated peak erosion. However, neither breach location overlapped with the observed breach that opened during Hurricane Sandy [62].

Breach dimensions during hurricanes are likewise difficult to quantify, though the growth of breaches over time has been documented [35, 55]. However, these studies address the days, weeks, or months following the storm. Initial breach size during a storm is less known. Lab and field experiments by Visser [65] for breaches in dikes are useful for providing a framework of initial breach growth, but the breach is initiated with a pre-drilled hole in the dike and does not simulate exactly what occurs to barrier islands during storms. Buynevich and Donnelly [7] performed a geologic mapping of some New England, USA, barrier islands and found geologic signatures to indicate the islands' past history with breaching and overwash.

They found ephemeral breaches with widths of 10–30 m before closing and breach depths of 1-3 meters below the dune crest. A few post-storm surveys have defined breach sizes before natural or forced closing. Kraus and Wamsley [35] discusses Pike's Inlet on Long Island, New York, USA, was initially 304.8 m wide and a nearby breach named Little Pike's Inlet post-storm had a 30.48 m width but over several months grew to over 914.4 m before it was closed. A breach near Moriches Inlet on Long Island studied by Schmeltz et al. [55] had an initial size of 91.4 m and 0.61 m depth. This breach expanded to 885 m with a three meter depth before it was mechanically closed. The uncertainties in breach dimensions and in where, how, and when breaches occur remains one of the many issues facing coastal communities today, due to the inability to predict or plan for the probable impacts of a breach forming where populations are highest.

Barrier islands exist along the coasts of 18 US states that border the Atlantic Ocean and Gulf of Mexico [70]. As coastal populations have increased considerably over the last few decades, the protective nature of barrier islands has become even more important [70]. The US National Hurricane Center (NHC) states that storm surge is the largest contributor to life loss and property damage during hurricanes [46]. During a hurricane, storm surge induces flooding that can damage structures, close roads, and impact the lives of communities living in the coastal zone. Storm surge can also speed up erosion on both barrier islands and the mainland coast, which then can drive more flooding. Understanding how barrier island breaching affects coastal flooding from storm surge is important for risk assessment and mitigation efforts. The opening of a hydrodynamic connection between the ocean and the back-barrier region can lead to increased flooding and waves during hurricanes that increase the risk to populations and property. However, there is little information currently available on how different breach morphodynamics affect the mainland.

1.1 Scope

The scope of this thesis is to aid in the understanding of how barrier island breaching during hurricanes impacts the back-barrier region and coastal inundation. Towards that goal, several factors need to be considered: Choosing a storm surge model to simulate hurricanes and the effect a hurricane has on the water levels near a barrier island system, how to appropriately isolate the impact of breaching from the complexity of the breach process itself, developing the tools necessary to perform a study on barrier island breaching with an ability to verify the accuracy of the solution, and lastly, analyzing the output of the results of the study itself. My study involved simulations of the Great New England Hurricane of September 1938 colloquially known as ”the Long Island Express” and the impacts barrier island breaching at Moriches, NY, may have on the adjacent mainland coastal region.

1.1.1 Organization

This thesis is organized into the following sections. Chapter 1 presents the introduction to the research performed herein. Chapter 2 presents a literature review of storm surge modeling and barrier island breaching. Chapter 3 is a discussion of the tools we created to be able to perform this study. Chapter 4 is a presentation of the results of this study, which are mostly extracted from an article under review at the Journal of Geophysical Research - Oceans. Chapter 5 is the conclusions and future work.

Chapter 2

Review of Literature

2.1 Storm Surge Modeling

Storm surge can cause widespread damage and death during a hurricane. In order to better inform risk and mitigation planning for at risk coastal communities, we first have to better understand the dynamics at play. Modeling of storm surge can aid in greater understanding of how storm parameters affect the surge and in how different regions respond. From a warning perspective, having accurate and fast predictions aid in evacuation plans in the days leading up to a storm's landfall. Storm induced flooding estimates are useful for city planner, risk management, and flood insurance estimates. The US has been estimating storm surge with different models for over 70 years.

2.1.1 Empirical Models

Early models created in the 1950s were empirical models that describe storm surge with a simple linear relationship between the maximum surge for an area with the central pressure deficit from the storm. These calculations were generated from data obtained at water level gauges and a linear best fit. The models created used separate calculations for the Atlantic and Gulf coastlines because the Gulf of Mexico exhibited a lower tidal signal, which changed how the storms interacted in that region [14, 26]. In 1957 Conner et al. [14] and Hoover [26] both developed very similar models around the same time that differed in the coefficient of variation used for the pressure differential's relationship to max surge. Conner et al. [14]'s ratio for storm surge to pressure deficit are for the Gulf of Mexico 2.1 and the Atlantic (2.2) coastlines.

$$h_{max} = 0.154 * (1019 - P_0) \tag{2.1}$$

$$h_{max} = 0.867 * (1005 - P_0) \tag{2.2}$$

where h_{max} is the maximum surge height for the location and P_0 is the central pressure of the storm. Hoover [26] calculated a best fit line that differs slightly from (2.1) and (2.2) both in the coefficient and also in which pressure was used to calculate the pressure deficit.

$$h_{max} = 0.151(1032 - P_0) \tag{2.3}$$

$$h_{max} = 0.198 * (1006 - P_0) \tag{2.4}$$

Hoover [26] also expressed that maximum surge follows a bell-shaped curve where the maximum for a particular storm and region is in one location and will decrease with distance,in both directions, from where the storm is making landfall. Both sets of equations employ a similar assumption that storm surge is directly related to a hurricane's change in pressure based on empirical observations of the time. Additionally, storm surge was consistently under-estimated when these equations were applied in a hind-cast of storms from which data was available. Early efforts at storm surge modeling were hampered by limited data and an underdeveloped understanding of how storm surge is generated by large storms and how the relationships between storm characteristics and local topography play a role. Harris [22] began to explore a multi-factored approach to the generation of storm surge and characterized the important inputs that go into surge generation in 1963. Harris [22] suggested that the use of computers in calculating these parameters will prove helpful in the estimation of storm surge. Harris [22] determined that there were five parameters that affected how storm surge is generated: pressure, direct wind, the earth's rotation, waves, and rainfall [22]. However, the lack of data from the structure of the wind fields in the open ocean hindered the efforts to clearly understand all factors in the generation of storm surge.

2.1.2 Computer based models

SPLASH

One of the first computer based storm surge numerical models was Special Program to List Amplitudes of Surges from Hurricanes (SPLASH), developed in 1972, [29]. SPLASH was developed to provide a forecast of the envelope of high water on a straight coast surrounding the projected landfall location. One output that SPLASH produced was a snapshot of the maximum surge for the basin of interest given the forecast storm parameters. Additionally, a correction factor was provided for changes in pressure deficit for every two millibars between +- 10 mbars from the forecast. A table of computed astronomical tide levels for the 12 hours before and after the landfall time was provided, with the assumption that the surge and tidal values could simply be added together to provide a total water elevation for that location. A complication of this model was that all values are given in straight lines and only applied to open water, no inundation was calculated. When the coastline is not a straight line, the model does not capture any local influence to the storm surge prediction. Additionally, the change in time and space of a hurricane forecast can influence the maximum and minimum surge values, depending on astronomical tide ranges. The understanding was that the forecaster can use the table of tidal values to update their prediction as the meteorological forcing was updated. SPLASH utilized a simple wind model for generating the wind inputs of the storm field. SPLASH provided a forecast of surge given idealized conditions; the storm parameters did not vary in space and time, and for an idealized open water coastline that is not curving.

SLOSH

The National Weather Service (NWS) updated their surge numerical model, in 1992, with Sea Lake and Overland Surges from Hurricanes (SLOSH) [31]. This finite difference model was developed to aid in storm forecasting efforts at the NWS National Hurricane Center (NHC). SLOSH brings more dynamic scenarios than SPLASH. Where SPLASH was only applicable in offshore open water and the coastline was treated as a barrier that cannot be crossed, SLOSH allows for coastal inundation, surge up rivers, estuaries, and bays. SLOSH employs a continuously varying polar coordinate grid that permitted finer resolution up rivers and estuaries and had the ability to contain sub-grid elements like barriers and channels. SLOSH incorporates current storm forecast data into the model to create the driving forces that generate the surge [30]; namely, the location of the storm, its central pressure, size and forward speed. SLOSH does not predict the storm's evolution, it only specifies the water's response to the storm inputs. Given the generation of the forces, SLOSH then solves the Navier-Stokes equations of motion at each point in the pre-defined grid for the region of interest to calculate the water's response to the storm forces.

SLOSH's grid was initially a polar coordinate curvilinear grid, but has since been expanded to include elliptical or hyperbolic grids [15] which is input as a mesh for the basins surrounding regions at higher risk for storm surge. The mesh has irregular spacing so that areas closer to the coast have a finer resolution than the deeper water. The grid spacing is still fairly coarse, ranging from 0.5 to 7.0 kilometers. SLOSH is computationally efficient and can be run quickly in response to storm track information. The numerical methods at the core of SLOSH were developed for 2D transport of the surge in response to parameterized wind and pressure forcing [20, 31].

SLOSH has several modes that can be utilized, first is the deterministic approach which is a single model run in response to storm best track information, which gives a forecast of one possible scenario. Second is the probabilistic approach which has been titled P-surge which is an ensemble forecast with each simulation based on the current best track forecast combined with past errors with National Hurricane Center forecasts. The errors are averaged and combined to generate a normal distribution, which is then sampled to provide a suite of 27 storm inputs that can be run to estimate many different forecasts. Lastly, SLOSH can be run in a composite approach, which is an ensemble of thousands of simulations with varying hypothetical tropical cyclone inputs. These simulations produce a maximum envelope of water (MEOWs) and the maximum of MEOWs (MOMs) and are utilized to determine storm surge vulnerability for the region in which the simulations are run [20].

SLOSH's main advantage is its rapid forecast based on continuously updated best track information. SLOSH can be run very quickly at a reduced computational cost than other storm surge models. SLOSH's pre-defined basins, while employing a variable resolution, are still quite coarse for identifying and accurately simulating smaller coastal features.

ADCIRC

The ADVanced CIRCulation model (ADCIRC) has a depth-integrated two-dimensional implementation (ADCIRC-2DDI) that uses the non-conservative form of the shallow water equations and has been used in past studies to model storm surge [41, 69]. ADCIRC is a finite element model that uses unstructured grids to allow varying resolutions across the study domain so that smaller scale coastal features can be resolved. Unstructured grids can also be very useful because they can be aligned with coastal features in ways that structured grids cannot [41, 69]. The use of unstructured grids also aids in basin scale domain sizes because allowing for a coarse resolution over areas of deeper water reduces the number of computations required and reduces the total computational requirements for the simulation [69]. ADCIRC-2DDI solves the non-conservative form of the shallow water equations with parameters for bottom shear stress, free-surface shear stress due to winds and obstructions, and momentum diffusion. ADCIRC can also employ a land roughness modification of the wind fields. There is a ramp up time in order for ADCIRC to properly model tidal and riverine forcing. One study required a startup time of 18 days prior to hurricane forcing to add in the appropriate tidal signal [69].

ADCIRC has many advantages over SLOSH because it has the capability of adding wind stress, tides, wave stress, and river discharge to its storm surge estimates. Additionally, ADCIRC's unstructured grids allow for much greater refinement at coastal regions, although this comes at a steeper computation time. A simple method of forecasting storm surge uses at least five hours of computation time under parallel processing conditions [60]. ADCIRC has additionally been used in an ensemble forecasting framework where a small subset of storm forecasts can be utilized to gain a suite of forecasts as each best track information was made available [18]. This setup was tested using a finite element unstructured grid of 77,000 nodes as an input domain with a resolution around 100 to 700 meters depending on location.

The advantage to using ADCIRC is that its solution has been validated to be relatively accurate for Hurricane Katrina [4] with a maximum surge error of approximately 1.2 feet. Additional validation for the tides and currents of Delaware Bay, with a small cm range of error for differing tidal constituents [4]. The North Atlantic Comprehensive Coastal Study (NACCS) performed validation on ADCIRC for several hurricanes, most notably Hurricane Sandy, Hurricane Irene, and Hurricane Isabel, and others with a good performance [11]. Disadvantages to using ADCIRC are the high computational cost from its large domain, early spin-up time, especially if adding in a tidal component, and the complexity of its input bathymetric mesh.

2.1.3 GeoClaw

GeoClaw is a more recently developed software package that solves hyperbolic differential equations in one and two dimensions to model geophysical events [2, 12, 40, 42]. GeoClaw is a module within Clawpack [3, 12] and employs adaptive mesh refinement (AMR) that allows for increasing resolution where and when it is needed and reduces the computational overhead while providing an accurate solution [3]. GeoClaw has been validated by the US National Tsunami Hazard Mitigation Program (NTHMP) for tsunami modeling. [21] describes the benchmarking process used to validate GeoClaw. GeoClaw calculates storm surge with a two-dimensional depth averaged model that solves the classical shallow water equations with source terms for fluid depth calculated from the bathymetry, bottom friction, Coriolis forcing, surface pressure, and wind friction (see Mandli and Dawson [41] for further details).

The adaptive mesh refinement employed by GeoClaw allows for high resolution at the coastline and coarser resolution in the ocean basins to reduce computational overhead during a simulation. AMR is a series of nested rectangular grids that can be aligned and layered such that solving across the grids leaves momentum conserved if mass is conserved [41]. Storm surge modeling with GeoClaw has been proposed to provide a robust but less computationally expensive model than ADCIRC [1, 41, 69]. Mandli and Dawson [41] compared GeoClaw with ADCIRC in a simulation of Hurricane Ike and verified the accuracy of the solution against in situ water level gauges that recorded data during the hurricane.

GeoClaw is open source, readily adaptable and has a lowered computational cost compared to ADCIRC and a greater ability to refine coastal features than SLOSH. Disadvantages of GeoClaw is that the default storm surge modeling does not provide tidal, riverine, or wave-stress calculations that are included in other models currently used in practice, such as ADCIRC [41, 69].

2.2 Barrier Island Breach

This section has been modified and expanded from Hoagland et al. [24] as our contribution to that review paper.

Overview of breaching

A breach is an opening in a narrow landmass such as a barrier island, dike, or spit that allows for a direct connection between two bodies of water [34, 35, 36, 66]. For a barrier island, this would be a direct connection between the ocean and the back-barrier bay or lagoon. Breaching is an involved process that can have an effect on the surroundings in which they occur. The negative effects of breaching can include loss of life, loss of navigability in adjacent inlets due to sediment being deposited, property loss from excess flooding, reduced access to property, habitat loss, increased repair costs for jetties and channel dredging [35, 36, 66]. Further effects on the local environment include increased salinity, and increased ocean wave exposure and stronger currents in the back-barrier region [35]. A breach in a barrier island can also cause existing inlets to close by longshore transport of sediment and diverting of currents to the breached area [36]. Additional consequences of unintended breaching include increased water level in the back-barrier region, which can increase flooding, and in turn increase erosion. A change in the tidal prism can also be caused when a breach occurs near an existing inlet or jetty and this tidal prism change can lower the channel depth which can reduce the ability to navigate the channel [35].

Breach Processes

High water levels near a barrier island caused by storms and heavy precipitation are among the primary drivers of breaching. There is a critical elevation for the water levels on either side of a barrier island that causes a gradient where the water will start to flow rapidly and erode the sediment of the island. This critical elevation may not necessarily involve inundation of the island, but erosion will still occur [35, 36]. Wave setup and storm surge raise the elevation of the water in both the ocean and in the back-barrier bay or lagoon. These higher water levels, combined with wave action from the swash and collision regimes, begin the erosion of the seaward side of the barrier island, reducing the stability of the dune slope [36, 49]. However, wave attack, by itself, while weakening the barrier dunes is unlikely to initiate a breach because the net erosion is seaward and does not push erosion landward [49]. Breaching can occur with two different transport methods, overtopping (overwash) and seepage and liquefaction [35, 36].

During the overwash and inundation regimes of storms, running water across the island can scour a channel between the sea and the back-barrier bay or lagoon [35, 49, 52]. Some duration of inundation and a strong flow are required for this scouring to occur. If the island has sections of low elevation, these sections can confine and intensify the scouring [35]. Breaching can occur from either the seaward and landward directions, but field data is limited in its ability to illustrate from which direction a breach is initiated [35, 49, 57]. However, Smallegan and Irish [57] shows that bay surge that comes after peak ocean surge is more likely to lead to breaching from the landward side of the barrier. This is due to peak ocean surge having already weakened the island through erosion caused by wave attack and swash [35, 57].

Breaching can also be caused by seepage through the barrier from high water levels in the bay. If the barrier island is narrow and high water levels in the bay are sustained long enough due to no ready egress into the ocean; seepage through the sediment of the barrier island can saturate and cause liquefaction of the sediment. These conditions allow sediment to flow very rapidly, creating a channel from the landward side of the barrier to the ocean and do not require the water to overtop the barrier[35, 36].

Visser [63] describes five phases of breach growth for sand dikes, which can be utilized to describe breaching of barrier islands as well. The first phase is erosion of the inner slope of the scour channel. Phase two is a decrease of the crest width. Phase three decreases the elevation of the crest. The fourth phase is called the critical flow phase; the flow through the breach is near critical and causes mainly widening of the breach. The final phase (phase five) is the sub-critical flow stage; this stage the flow is small enough that only widening occurs and eventually erosion virtually stops when the water levels equalize on both sides of the barrier. During the phases of breach growth the cross-shore transport of sediment is much greater than longshore transport, but once equilibrium is obtained longshore transport dominates and could cause closure of the breach [36].

Factors that determine whether breaching will occur and where include the storm conditions and the topography of the barrier island. Barrier islands that have a larger volume with a higher dune peak above mean sea level (MSL) minimize the likelihood of a breach occurring [35, 36, 49]. In such cases, the width and height of the island allow it to withstand wave attack and avoid inundation [36].

There is a limited number of studies which document barrier island breach dimensions. The lack of data makes it difficult to quantify how breaches evolve during a storm. Lab experiments and field experiments by Visser [64] for breaches in dikes are useful, but the breach is initiated using a pre-drilled hole in the dike and does not simulate exactly what occurs during storms on barrier islands. Buynevich [6] performed a geological mapping of some New England barrier islands and found geologic signatures to indicate the islands' past history with breaching and overwash. They found ephemeral breaches contained widths of 10-30 m before closing and depths of 1-3 m below the crest of the dune. Past history of inlets showed that these breaches widen over time to 100-600 m and depths up to 4 m. A few post-storm surveys have defined breach sizes before natural or forced closing. Kraus and Wamsley [35] discusses Pike's inlet on Long Island, NY was initially 304.8 m wide and a nearby breach named Little Pike's inlet was initially 30.48 m wide but over several months grew to over 914.4 m before it was closed. A breach near Moriches Inlet studied by Schmeltz et al. [54] has an initial size of 91.4 m and 0.61 m depth. This breach expanded to 885 m with a 3 m depth before it was closed by the United States Army Corps of Engineers (USACE).

To gain an understanding of how long it takes to open a breach during a storm, we would need data that is difficult, if not impossible, to obtain of the sediment transport during the storm. The intense hydrodynamic action of a storm would most likely damage instruments, and there is no guarantee instruments could be placed precisely where a breach will occur. Indeed, some modeling efforts to simulate breaching during specific storms have modeled breaches that are similar to what occurred but not in the exact locations [8, 61]. Because the timing data is sparse, we need to use simulations and experiments to gain an understanding of the timings involved in breaching. Visser [64] performed an experiment on breach growth in sand dikes and found the rate of lateral breach growth is approximately 2 cm/s. Roelvink et al. [52] simulated this experiment in XBEACH, a wave propagation and sediment transport model, and found results consistent with Visser [65]. Kraus and Wamsley [35] references a 'certain duration of inundation' before breaching will occur, but this process depends on the forcing conditions and the baseline topography. Harter and Figlus [23] shows that breaching occurred during the 10 hours of inundation of Hurricane Ike, but no further definition of how long the breach took to open is provided. de Loof et al. [17] found during experiments on breach growth in sand dikes that breaching starts when the water velocity in the breach reaches greater than 1 m/s. Additionally, the relationship between the size of the dike crest was found to influence how quickly a breach occurs. Narrow or lower dike crests breach much more quickly than a dike with a higher or wide crest [17]

2.2.1 Barrier island morphodynamics models

Modeling of barrier island breach is a complicated process because the factors involved in breaching are also complex. Two current models have been developed to gain a better understanding of barrier island dynamics during storms. XBEACH (eXtreme Beach) and CSHORE (cross-shore numerical model) [32, 52]. Both of these tools are physics based models that combine wave action, sediment transport, roller energy, and swash zone processes. XBEACH is a 2D horizontal (2DH) model that allows for alongshore variability, while CSHORE is a 1D model that assumes a uniform barrier island [32, 52].

XBEACH

XBEACH applies physics based equations for differing portions of barrier island morphodynamics using the regimes as outlined by Sallenger A.H. [53] [52]. For the swash regime the model uses a 2DH wave group and infragravity wave forcing also combined with a roller model to use for momentum in surface rollers. For the collision regime the models adds a sediment transport component that allows for a dry to wet area avalanching model, which assumes wet material transports more easily than dry material, and slumping caused by infragravity runup on the dry dune. The overwash regime uses flow that is controlled by the low frequency motions on wave-group timescale [52]. XBEACH was validated using lab experiments in both the 1D and 2DH modes, as well as field cases. The validations found that

XBEACH performs well with some overestimation of the wave energies and dune reduction being simulated.

Studies using XBEACH include [19, 56, 57, 61]. Frey [19] used XBEACH to calculate dune lowering using 4 idealized storm scenarios. They verified that dunes which had a lower elevation at the onset of the storm were reduced more during the storm conditions than higher elevation dunes. Additionally, they found that narrower portions of the barrier island were more vulnerable to breaching than wider areas. Sherwood et al. [56] was able to compare pressure sensor data from hurricane Ike to XBEACH model results of the same hurricane. They found that the modeled water levels results closely matched that obtained by the pressure sensors. The model showed similar overwash channels as were observed after the storm passed, but the model overestimated the elevation change [56]. Smallegan and Irish [57] performed a sensitivity analysis using XBEACH to determine how much barrier island change relies on the timing between peak bay and ocean surge. The model predicted that for some locations, the timing of the bay surge coming after ocean surge was extremely important to the amount of change the island experienced. van der Lugt et al. [61] studied the predictive capability of XBEACH by calibrating it for one storm and applying it to two different locations and storms. They found the model performed well for predicting dune lowering, erosion, and deposition of sediment. Breaching was also predicted by the model, but not in the exact locations as occurred during the storms.

CSHORE

CSHORE stands for cross-shore numerical model and was developed by USACE in response to an increased need for greater understanding of beach morphology in order to predict and mitigate damage during storms [32]. CSHORE is a wave current model that combines cross and longshore momentum, wave action, and roller energy equations. The purpose of this model is to more accurately model the beach profile reactions to storm forcing. CSHORE has been compared with lab experiments and extended to better predict overwash, erosion, and deformation [32]. CSHORE is based on an assumption of longshore uniformity and is a tool that can best be used in idealized case studies. CSHORE does not include any inundation simulation and as such does not model breaching of barrier islands, beyond direct sediment erosion through wave action [23].

Harter and Figlus [23] provides a comparison of XBEACH and CSHORE simulated morphodynamic changes of Follet Island after hurricane Ike. XBEACH was able to accurately predict the flow areas affected by the hurricane and shows several breaches that align with post-storm LiDAR data. XBEACH was overall more accurate than CSHORE but took significantly longer to process. CSHORE being a 1D model runs more quickly but less accurately, as it was unable to predict breaching. CSHORE could accurately simulate the shoreline and slope of Follet Island after the hurricane passed.

Modeling Barrier Island Breach

In order to accurately model the processes that drive barrier island breaching, there are many factors to consider. Firstly is timescale, choosing a model that either simulates breaching using short term outcomes, as in barrier island direct response to storms. This would need results that are on the timescale of days. Or when longer time-scales come into play, looking at barrier island breach evolution beyond the initial breach formation. There are studies that have attempted to accomplish both the short and long term time scales. KRAUS and HAYASHI [34] employed a morphodynamic model aimed at longer term time scales. The model was initially validated with a dike breach experiment by Visser [64] to record the sediment transport timing of the initial breach. They then modeled an actual breach near Moriches Inlet from 1980 to gauge if the model reproduced how large the breach evolved over several months before it was forcibly closed. Cañizares and Irish [8] were more specifically interested in shorter time scales, the barrier island's direct response to storms. They examined two historical storms that produced extensive flooding and breaching, and their simulations were on the order of hours instead of months to examine if the model faithfully reproduced flooding and breaching that occurred during these storms. The commonality behind both approaches [8, 34] is in the model frameworks. Complex hydrodynamic models were combined in an effort to simulate sediment transport, wind and wave forcing, storm surge and island inundation. For Cañizares and Irish [8] this involved a combining an offshore wave model (WISWAVE) a sediment transport model (SBEACH), storm and water level model (ADCIRC) and bay water level and nearshore wave model (DELFT3D). Combining the differing physics-based models allows researchers to perform simulations for an accurate estimation of the dynamic changes a barrier island undergoes during a storm.

Overall a combination of different numerical models is useful for providing all the information. A large scale storm model like ADCIRC to produce the wind and wave forcing can be fed into a more localized model like XBEACH, where that forcing can specifically be used for simulating the barrier island response.

Chapter 3

Methods

Our overarching goal was to perform an analysis of how barrier island breaching impacts bay flooding and coastal inundation with many simulations to gain a statistical agreement of the maximum surge in the bay and mainland inundation. To accomplish this goal, we had to piece together many different concepts and ideas to perform the simulations. These methods have been expanded and adapted from two manuscripts submitted from review to Journal of Geophysical Research - Oceans and Journal of Open source software.

3.1 Study Area

We chose to study Moriches, NY, a section of the barrier island that spans Long Island, New York, along the Atlantic Ocean. Moriches Bay is in between Great South Bay, to the west, and Shinnecock Bay, in the east, as part of the same barrier island system. This region is heavily populated and is impacted by storms regularly. It was especially damaged by the Great New England Hurricane of 1938. The barrier island runs roughly parallel to the mainland at Moriches Bay and is comprised of two segments of a larger barrier island system. This system spans the southern portion of Long Island, NY. Fire Island, the center island in this system, connects to Westhampton Beach via Moriches Inlet and is the portion of this barrier island system we studied. This segment of the barrier system is approximately 20 kilometers long with a width that varies from 0.25 to 0.50 kilometers between the ocean and the bay and has a dune height of approximately zero to nine meters above mean sea level (MSL) [16, 39]

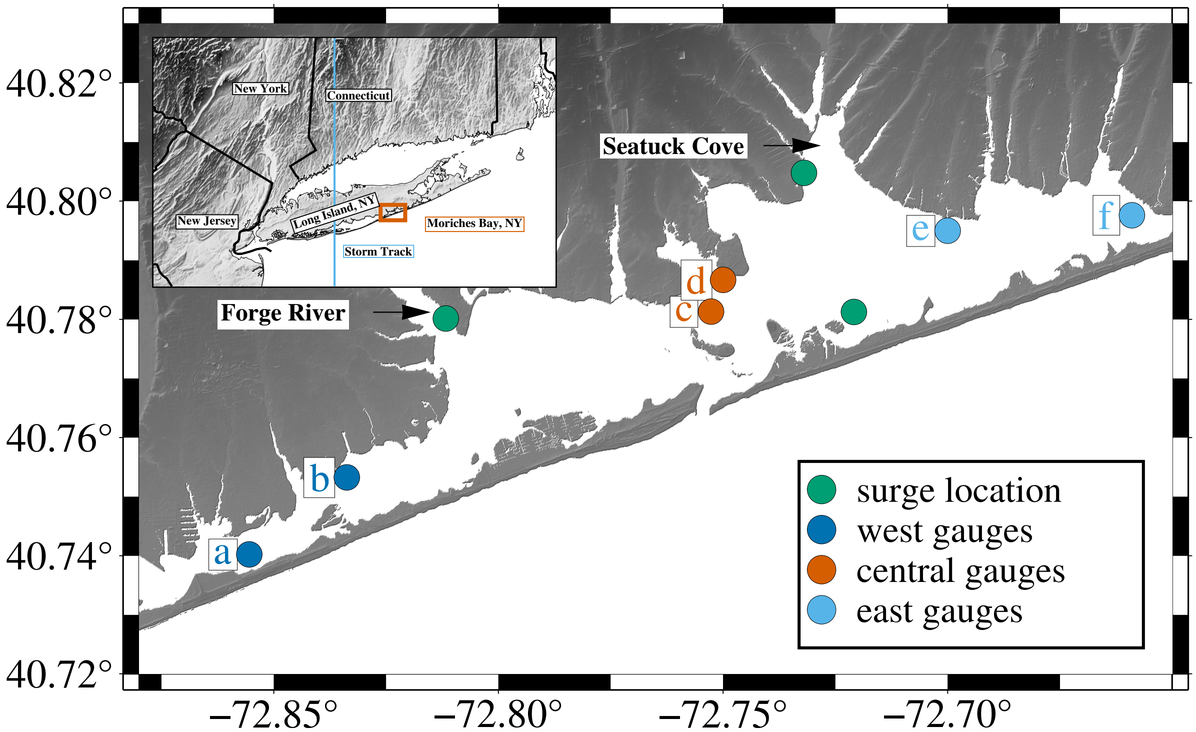

Figure 3.1: Map of study area Moriches, NY. Inset shows region surrounding Moriches NY, (orange box). The light blue line is the track of our simulated storm, a proxy for the 1938 Hurricane. The green circles are locations of surge measurements displayed in Figure 4.2, and the remaining circles are locations of synthetic water level gauges illustrated in Figure 4.1

3.2 1938 Hurricane

The 1938 Hurricane was a storm that made landfall as a category 3 hurricane near Moriches, NY, on September 21, 1938. The center of the storm passed over the western side of Great South Bay, less than 75 kilometers from Moriches Bay. Figure 3.1 illustrates the location of Moriches Bay, NY, and the storm track's location as it made landfall. It generated 10 breaches across the entire barrier island system bordering the south shore of Long Island, NY, and caused widespread damage [8, 13, 44]. Six breaches were opened during the hurricane at Moriches, NY, three west of the inlet and three east of the inlet. We chose to use this hurricane to provide the storm forcing for our study because its documented breaches lend realism to the simulations and there is one National Oceanic and Atmsopheric Administration (NOAA) tide gauge that has data recorded from this storm that can be used to validation of the model's simulated results [9].

3.3 Numerical Model

Choosing a numerical model was an important step in this study. SLOSH provides the ability to run many thousands of simulations at low computational overhead, but the coastal resolution is large at 1-4 km between nodal points. ADCIRC can be coupled with a morphological model for the complex part of breaching and includes tides and wave effects as the model output. However, ADCIRC's computational needs are extensive and would limit the number of simulations that we could run over the course of this study. GeoClaw provides the AMR to make resolving the coastline more flexible and less computationally intensive. Additionally, the open source nature of the code allows for making changes to the model itself to provide a more flexible way to generate the breaching at the core of this study. For the purposes of solely studying the impact of breach dimensions and locations on mainland flooding, we did not seek to add tidal, or wave induced surge to my simulations, which also simplifies the simulations so that more can be run with less resources.

3.3.1 GeoClaw - Breaching implementation

Breaching is a complex process that is difficult to accurately model. Storm forcing combined with barrier width, sediment transport, and other complex processes make it challenging to predict where and when a breach will occur. There is a lack of studies that document barrier island breach dimensions during storms. Due to the nature of storm induced breaching, it is difficult, if not impossible, to quantify what exactly occurs to create a breach in a barrier island during a hurricane. Lab studies of breaches in dikes provide some clues into breach formation [65]. Studies that map breach locations and dimensions usually occur well after the storm. This delay in quantifying breach dimensions does not help define initial breach width and depth, as breaches will continue to grow as water passes between the ocean and back-barrier region.

To accomplish our goal of quantifying flooding due to breaching, we chose to simplify breaching by reducing the topographic elevation of the barrier island at specific locations. We created an algorithm inside one of GeoClaw's modules that allows new conditions to be added to the simulation. This allowed the topography of the barrier island to be reduced over time during the simulation. We imposed a Gaussian bell-curve onto the topography at specific pre-defined locations at times near landfall, when the peak ocean surge is highest. Equation (3.1) was embedded into the simulation where d^t is the dune height at the current timestep d^{t-1} is the dune height at the prior timestep, X is the alongshore coordinate currently being reduced, μ is the alongshore coordinate at the center of the breach area, and t_T is a timing factor that controls how quickly the breach opens.

$$d^t = d^{t-1} - e^{-\frac{1}{2}(X-\mu)^2} t_T \tag{3.1}$$

For each patch of AMR that GeoClaw calculates, it loops over the patch coordinates until the selected location is found and then begins to reduce the dune height until the next timestep and repeats until the final depth is achieved. The goal of using a Gaussian function was to achieve a breach that has sloping sides and is deepest at the center. The timing factor for these simulations allows for the breach to open fully in an hour after the experiments performed by Visser [65] and was calculated using Equation (3.2). This equation is simply the number of seconds between subsequent time steps divided by the number of seconds in one hour.

$$t_T = 7.57/3600 \tag{3.2}$$

The calculation to reduce the dune height is controlled in the cross shore by the latitudes that are the transition between land and water for the bay and ocean. Figure 3.2 is a schematic to illustrate equation (3.1).

3.3.2 GeoClaw - Storm Forcing

GeoClaw's storm surge simulation requires the accuracy of best track data from sources like HURDAT [38], which provides a time series of the storm's evolution as it travels towards North America. Key metrics include the radius of maximum wind (RMW), pressure radius, pressure deficit, and eye location. From this data several different algorithms can be used to calculate the wind and pressure fields that generate the storm surge, the most frequently used being Holland [25]. However, the 1938 hurricane's best track information is sorely lacking in this data, instrumentation at the time was not adequate to obtain it and reconstructions based on statistical calculations are difficult to obtain. The USACE North Atlantic Comprehensive Coast Survey [10] contracted a company to generate thousands of synthetic tropical cyclone wind and pressure data that were based on statistical sampling of historical TC. These datasets were generated for USACE from a planetary boundary layer

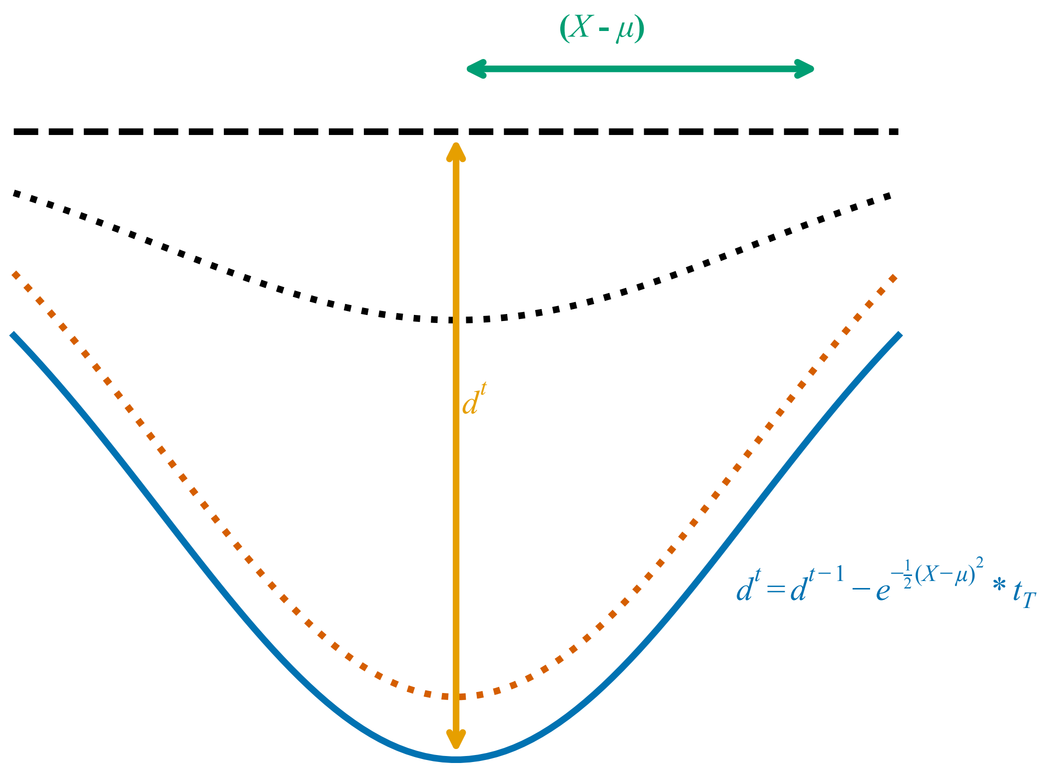

Figure 3.2: Schematic of breach growth based on equation (3.1) (X - μ) is width of breach for each location lowered. d^t is total dune height at the center of the breach. Black dashed line indicates original barrier dune height. Black dotted line indicates breach growth at an intermediate time t. Orange dotted line is breach growth at nearly final time t. Blue line is final breach.

(PBL) model, which utilized six storm parameters: the storm track, the heading direction, the central pressure deficit, the radius of max winds, and the translational speed. Each parameter was sampled from historical tropical cyclones from National Oceanographic and Atmospheric Administration (NOAA) National Hurricane Center HURDAT2 (HURricane DATa 2nd generation) [38] database and then were used to generate probability distributions. The probability distributions provided combinations of parameters that were input into the planetary boundary layer model, which calculated the wind and pressure data for use in simulations. The wind and pressure data were validated post simulation using several historical hurricanes and given an uncertainty of 0.39 meters for the region covering New York and New Jersey [45]. The USACE shared with us ten of these synthetic TC datasets that aligned with the track of the 1938 Hurricane. The caveat is that GeoClaw was unable to utilize such inputs at the time.

We chose to make additions to GeoClaw that would allow wind and pressure data to be used during storm surge simulations as part of our study, as it had been informally requested by the USACE and others over the years since GeoClaw's storm functionality was implemented.

3.3.3 GeoClaw - model development

GeoClaw's adaptive mesh refinement posed several challenges for running storm simulations. The data must be in format that is able to be read by the FORTRAN code, and then the data must be interpolated in time and space so that the forcing conditions can be advanced as the storm progresses. The NACCS wind and pressure data was generated for 15 minute increments at a 0.25 degree spatial resolution. This spacing and timing works for the initial forcing in the Atlantic basin, but as the storm approaches the coastline, the simulation needed increased refinement to accurately evolve the storm surge calculations for a greater understanding of coastal changes. GeoClaw's current storm forcing generation uses wind and pressure models like Holland [25] that calculates the radial profile of wind and pressure and expands it in a circular domain to generate the initial conditions for generation of storm surge. The NACCS synthetic storm data is already in these wind and pressure fields but needed to be converted to a standardized format for reading in both FORTRAN and Python. Utilizing a commonly used netcdf4 binary format was beneficial because it is a standardize scientific format that can be utilized with multiple programming languages, in this instance both Python and FORTRAN. The storm forcing data was in two sets of files, a wind field file and a pressure field file. Each file contained arrays of data that covered a rectangular domain within the Atlantic Basin, and in a fixed width format. The wind data was in the format of the wind velocity in the x direction followed by the wind velocity in the y direction. We wrote a python class that opens the files, reads in the wind and pressure data for all timesteps and then parses the arrays to organize them per time step. For each time step, the total wind velocity was calculated from the individual components of the wind u being the wind velocity in the x direction and v the wind velocity in the y direction. We calculated the location of the eye of the storm as the minimum central pressure in the pressure arrays. The output of this processing is a single file in a nested array structure where each time step includes the components of the wind, the total wind speed, the pressure, the eye location, and the array locations; where each data point has a specific location in latitude and longitude. This file format can be easily processed with both Python and FORTRAN (see Jeffries and Mandli [28] for code).

The FORTRAN at the core of GeoClaw's calculations requires that the forcing is read into the model at the start of a simulation. Because GeoClaw allows the use of multiple forms of best track input we added a flag to signal to the program that a data derived storm input was being used. This enabled the program to use a different data parsing routine for the storm parameters. Once the data was read into memory, the calculations can begin. For each patch of AMR, at each time step, the data needs to be interpolated from the coarse grid to a smaller, more refined grid. The data was originally provided in 15 minute increments, but AMR and the storm surge estimation are in sub-minute increments. We used a linear interpolation scheme to calculate the values for the components of the wind speed and pressure values for each time step generated by GeoClaw. The linear interpolation equation is as follows:

$$\begin{aligned} weight &= \frac{t - t_{n-1}}{t_n - t_{n-1}} \\ x &= (x_n - x_{n-1}) * weight + x_{n-1} \end{aligned} \tag{3.3}$$

where t is the current time step, t_n is the index of the closest data point, and t_{n-1} is the last data point from the original file, x is the current data point being interpolated whether it is wind in the x direction, wind in the y direction, or pressure. x_n is the nearest value from the original data and x_{n-1} is the previous data point.

Once the adjustment to the current time step has been made, the data needs to be interpolated spatially as well. For each increment in time the storm is moving, but the gaps between the 15-minute increments are too large for the continuous scale produced by GeoClaw. We used bi-linear interpolation of each data point whether wind or pressure in equation (3.4).

$$\begin{aligned} f(x, y_1) &= \frac{x_2 - x}{x_2 - x_1} * f(x_1, y_1) + \frac{x - x_1}{x_2 - x1} * f(x_2, y_1) \\ f(x, y_2) &= \frac{x_2 - x}{x_2 - x_1} * f(x_2, y_1) + \frac{x - x_1}{x_2 - x_1} * f(x_2, y_2) \\ f(x, y) &= \frac{y_2 - y}{y_2 - y_1} * f(x, y_1) + \frac{y - y_1}{y_2 - y_1} * f(x, y_2) \end{aligned} \tag{3.4}$$

See Figure 3.3 for a visualization of this algorithm. This calculation is repeated over the course of the entire simulation at every time step and AMR patch created. Interpolation of the data increases the potential for errors in the solution, so the ability to test the program's storm surge estimation is important.

We validated this new functionality to GeoClaw by taking an example storm surge simulation for Hurricane Isaac and ran the simulation with the original inputs. We then converted the storm track data into wind and pressure fields that were in the same format as the NACCS data we received, and ran a new simulation with this data derived storm inputs. Figure 3.4

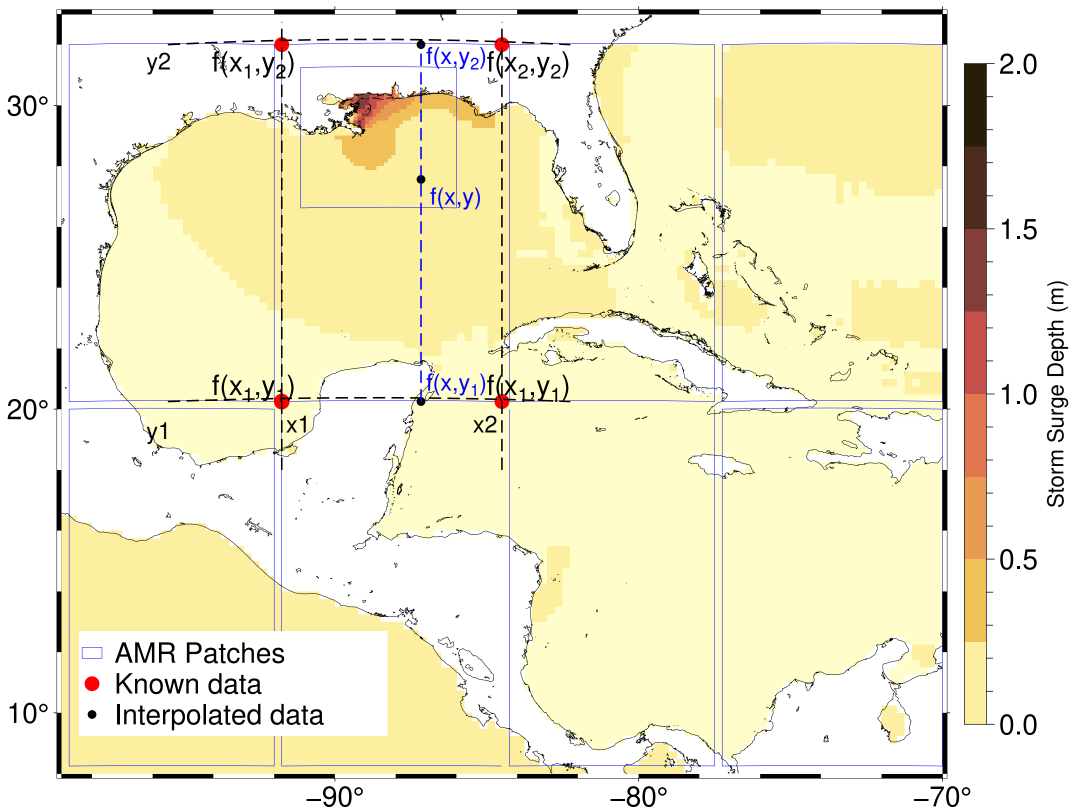

Figure 3.3: Visualization of spatial interpolation of storm data. Pictured is the storm surge estimation for Hurricane Isaac at the time of landfall, blue boxes are the AMR patches created by GeoClaw, red circles are points already defined by storm data, blue circles are interpolated data points

is a comparison of Hurricane Isaac near landfall with the original (top) and data derived wind fields (bottom).

The wind and pressure fields are a reasonable match but do have some differences with the wind being more oblong towards the outer edges because of inaccuracies within the bilinear interpolation algorithm's estimation near the edges of the wind and pressure fields. This oblong shape can be reduced with a smoothing parameter but does reduce the solution's accuracy because the smoothing parameter is dependent on an estimation of the pressure radius within the storm which is not easy to estimate. Adding the smoothing parameter in a few tests reduced the maximum surge by an amount that varied on which background

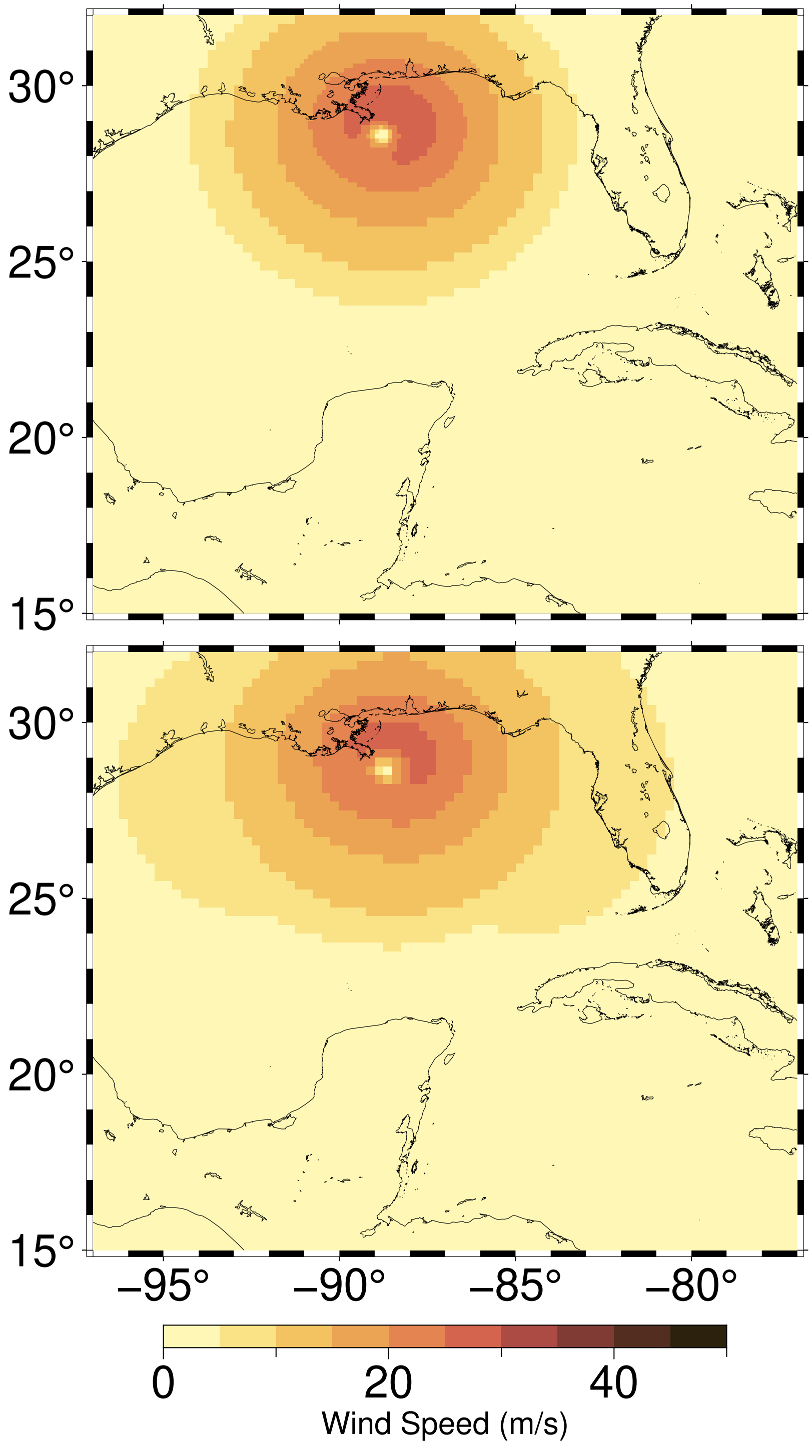

Figure 3.4: Comparison with wind fields generated by best track inputs and Holland (1980) wind field generation with data derived additions to GeoClaw using bi-linear interpolation. Top panel is the original storm generation built into GeoClaw, bottom panel is my added functionality resultant wind field.

pressure was used to identify the pressure radius. This addition to GeoClaw can be found as a open pull request to the GeoClaw main Github branch and will be integrated into the full package in the near future [28].

3.4 Study Methods

3.4.1 Storm Forcing

The storm we employed to simulate storm surge is a proxy for the 1938 New England hurricane. The selection of synthetic tropical cyclone data we received from the USACE included ten storms that most closely resembled the track of the original hurricane. To choose which storm was a closest approximation, we ran simulations of all ten storms and compared the results of these simulations with data that was recorded at a water level gauge at Sandy Hook, NJ (Station ID: 8531680) during the original hurricane. The closest matching storm's (storm number 486) maximum surge arrives a little bit earlier than the actual data but does otherwise show a reasonable agreement. Figure 3.5 is a comparison of all ten storms against the data from the NOAA gauge. The original data recorded during the hurricane is referenced to local mean sea level of the time, and in which we removed the tidal component. We adjusted the data 0.239 m to match the modern datum used by NOAA [9] which accounts for sea level rise at that station. Our synthetic water level gauge data produced by GeoClaw is calculated with bathymetry that uses NAVD88 as the vertical datum, which is 0.073 m above the local MSL for Sandy Hook. We reduced the synthetic gauge data to bring both the synthetic and original data to the same datum.

The storm approached Long Island, NY from directly south. The track is illustrated with a blue line on the inset of Figure 3.1. As the storm approached, storm surge seaward of the

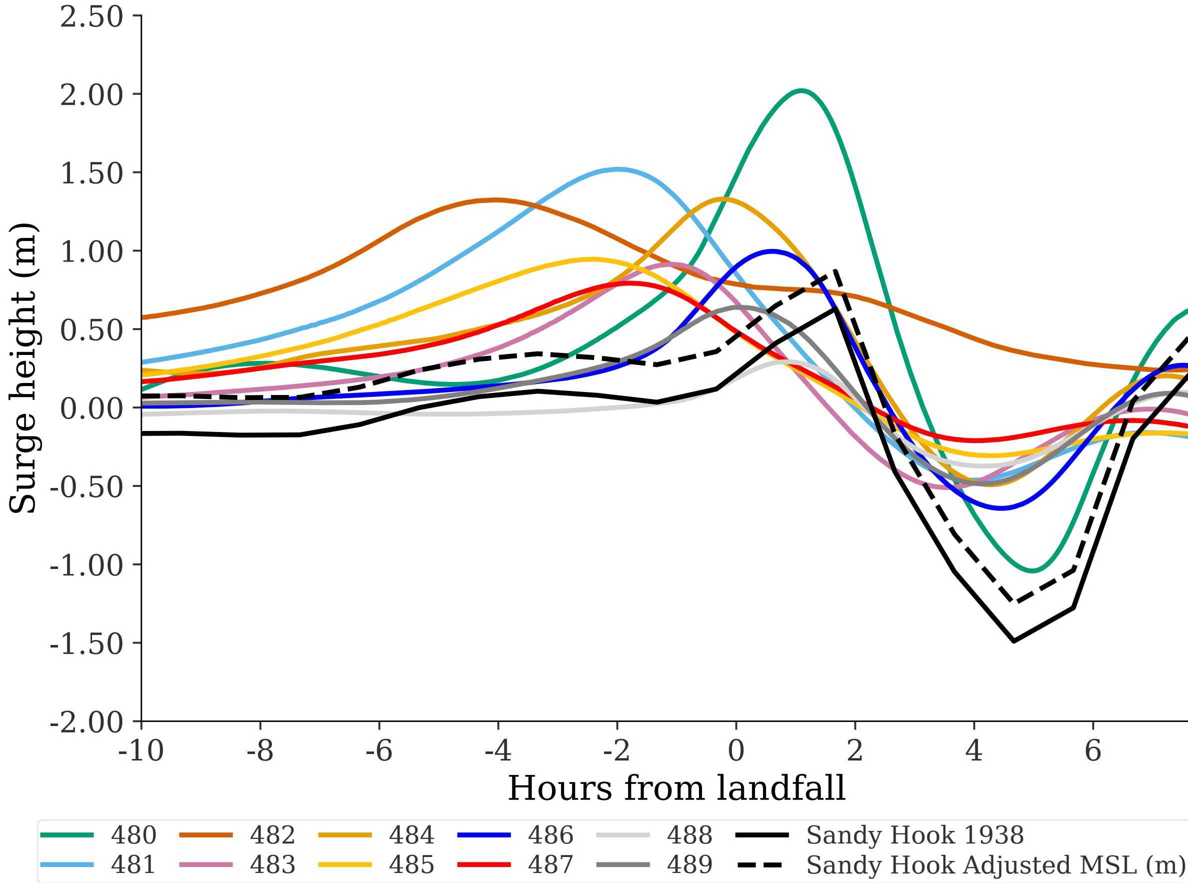

Figure 3.5: NOAA water level gauge data from the 1938 hurricane compared with simulated water level gauge data at Sandy Hook, NJ for all synthetic storms. Black line is original data before adjusting for modern mean sea levels. Dotted black lines are the data adjusted 0.239 to match the datum used by NOAA. All other lines are for 10 storms simulation output adjusted -0.073 for the difference between NAVD88 and local MSL.

barrier island began to rise from southwest to northeast starting approximately 18 hours before landfall. The timing of the peak ocean surge varies along the barrier island, with the peak occurring in the northeast approximately ten minutes after it arrived in the southwest. This peak surge occurred within minutes of landfall. Inside the bay there was a local wind setup from northeast to southwest prior to landfall and after peak ocean surge the surge is pushed into the southwest of the bay from the connection to Great South Bay. As the storm continued north, a small setdown occurred three hours after landfall inside the bay.

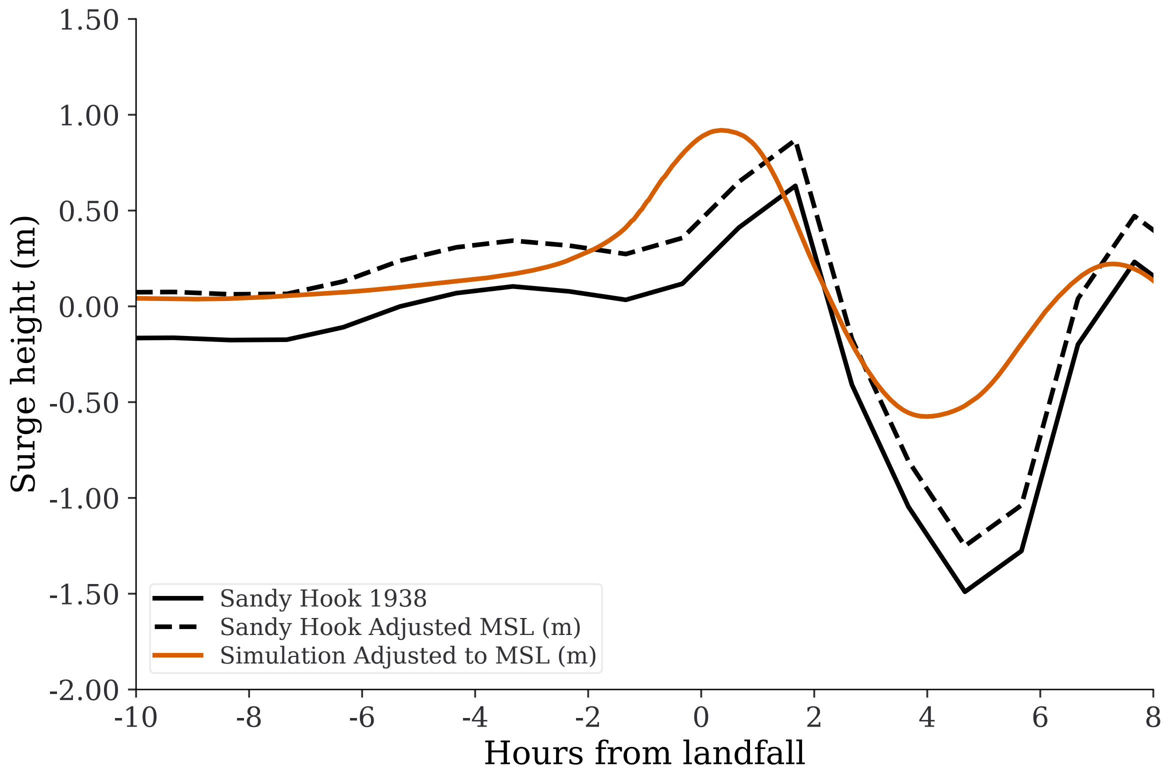

Figure 3.6: NOAA water level gauge data from the 1938 hurricane compared with simulated water level gauge data at Sandy Hook, NJ. Black line is original data before adjusting for modern mean sea levels. Dotted black lines are the data adjusted 0.239 to match the datum used by NOAA. Orange line is the simulation output adjusted -0.073 for the difference between NAVD88 and local MSL.

3.4.2 Simulations

We set up our simulations with a basin scale bathymetry using GEBCO 30 arc second [68] for the region that spans 98W to 57W and 5N to 45N with a maximum AMR of 6750 meters in each direction. We obtained bathymetry for Moriches, NY, from NOAA's continuously updated 1/9 arc second topobathy dataset [16]. We specified GeoClaw's AMR for Moriches Bay and its adjacent barrier island to be a grid of 18 x 18 meter cells, which was the smallest resolution we could obtain while balancing computing time. The refinement began well before the storm arrived to more accurately simulate the surge as it enters the bay. We placed synthetic water level gauges dispersed through the bay in the same configuration that was used for the NACCS project maximum surge locations [10] and a series of water level gauges on the seaward side of the barrier every two kilometers that we used to verify nearshore surge height for breach initiation.

To create a baseline for quantifying the flooding and inundation changes in different simulations, we ran a no breach scenario. This was necessary to see how the storm impacts the barrier island, bay, and coastline in this storm event and in the absence of breaching. The water level gauges we placed in the bay and at the seaward side of the barrier island are useful for discerning differences in surge height and timing when compared to the rest of the simulations.

To gather an understanding of how different breach scenarios impact surge and inundation, we ran several categories of simulations that varied the width, depth, location, and numbers of breaches. For my first grouping of scenarios, we used the original breach locations formed during the 1938 Hurricane. We estimated the original breach dimensions from observations reported in Cañizares and Irish [8] and references therein. The locations specified use a single longitude as a center point (μ) from Equation (3.1). We used the latitudes that touch the bay and ocean that are directly north and south from μ. We created a Monte Carlo framework that employs a random, uniform distribution for each individual breach's width and depth. The time of initiation for each breach was chosen using the the no breach simulation results for the nearest synthetic water level gauge data seaward of the island; the first time in seconds that the nearest water level gauge reaches 24% of the maximum dune height at each location was our breach initiation time. Due to variations in the barrier island topography from 1938, the dunes at the original breach locations are much higher, rather than adjusting the topography we used a threshold of offshore surge height to initiate breaching. The maximum surge we found to breach all six locations was 24% of the dune

Table 3.1: Breach input data for the 1900 simulations for our study. Each category of simulation's widths and depths were chosen by Monte Carlo methods using a random uniform distribution between endpoints identified from literature

	Num. Simulations	Num. Breaches	Min. Width	Max. Width	Min. Depth	Max. Depth
Width Simulations	464	6	25.00	628.97	-2.00	-1.00
Depth Simulations	424	6	110.40	627.90	-2.02	-0.00
Width and Depth Simulations	297	1 - 5	25.00	628.97	-2.02	-0.00
Locations	315	1 - 294	25.00	629.00	-2.01	-0.00
East of Inlet	193	1 - 99	25.00	629.00	-2.01	-0.00
West of Inlet	200	1 - 99	25.00	628.99	-2.01	-0.00

heights under our chosen storm reconstruction. Additionally, we chose to have the breaches fully open within one hour after initiation after Visser [65].

We created six broad categories of simulations as illustrated in Table 3.1, *Width*, *Depth*, *Width and Depth*, *Locations*, *East of Inlet*, and *West of Inlet*. In *Width* we randomized the width of the breaches, keeping the depth steady at -2.0 meters below mean sea level and using the original six breach locations that occurred from the 1938 Hurricane. Each breach used boundary values between 25 meters and 630 meters, these limits are the few details on initial breach size found in the literature [8, 35, 55, 65]. For the *Depth* simulations, we kept the original 1938 breach width estimations and varied the depths between 0 and 2.0 meters below mean sea level. The widths were estimated in Cañizares and Irish [8] and references therein. *Width and Depth* we randomized both dimension parameters, but also varied the number of breaches from one to five. Each breach in the *Width and Depth* scenarios occurs at one of the original locations, but which breach location was randomly chosen. Lastly, the *Locations*, *East of Inlet*, and *West of Inlet* category we varied all of the breach parameters, from numbers of breaches, the dimensions of each individual breach and where the breaches occur along the island. For the *Location* category, our Monte Carlo framework selected an alongshore coordinate from a list of values that span the entire barrier island. For the *East* and *West* categories, we limited the breach locations to coordinates to sections of the barrier island on either side of the inlet. Once the alongshore coordinate was chosen, our algorithm then verified that the maximum surge height at the nearest ocean water level gauge reaches 24% of the maximum dune height. This criterion assumes that the location can be inundated. If no gauges within two kilometers of the chosen location reach that threshold, we started over with a new location. This allows for a reasonable estimate of the conditions that could induce breaching. If the water levels just offshore do not reach that critical elevation, it is assumed to be unlikely that a breach would open at that location. We constrained the maximum number of breaches by using our nearshore surge height of 24% of dune height to provide a count of how many locations are viable. With these criteria, we found that there was a maximum of 295 individual breach locations possible for this particular storm along the length of the island. For the *East* and *West* simulations, we limited the number of breaches to be less than 100 per section of the island. Determining that there are 295 locations that fit our ratio of dune height to offshore surge height illustrates the non-linearity and stochastic nature of the processes that lead to breaching, given that in 1938 only six locations breached during that hurricane.

3.4.3 Data Analysis

We evaluated my results using the total horizontal inundation along the mainland coastline, and maximum surge height data recorded by GeoClaw for the entire bay, at specific points within the bay (green circles on Figure 3.1), and the surge time-series generated at select synthetic water level gauges (blue and orange circles on Figure 3.1).

Water Level Gauges

GeoClaw records time series data from the synthetic water level gauges at five minute intervals during the storm simulation. We gathered the data from my synthetic water level gauges for each portion of the bay and calculated the mean, median, 5th and 95th percentiles of each category of simulation to visualize trends in the different categories across the surge timing and locations. This data allows us to see local changes such as wind setup and setdown if it occurs where that water level gauge is located.

Inundation

We calculated inundation differences by first identifying the grid cells that were above mean sea level in the bathymetry (dry cells) which were inundated (wet cells) in our baseline scenario, which had no breaching. We used these wet cells to then identify the changes in inundation for each simulation. The change in wet cells from our baseline scenario allowed me to see differences in inundation that were directly caused by breaching of the island. Each cell is an 18x18 meter square which provides a total area of 324 square meters. We obtained this data by using GeoClaw's fgmax functionality, which tracks the maximum surge in each cell of interest and continuously updates the values until it reaches a maximum. The maximum surge and inundation are snapshots in time and do not allow for dynamic analysis as in the synthetic water level gauge data.

Bay Surge

To evaluate bay surge, we divided the bay into thirds; west, central, and east and used our recorded maximum surge data to look at specific locations for each section of the bay to create distributions of the surge per simulation category. We also analyzed the maximum surge for each section of the bay in total. Lastly, we took the total maximum water height and created maps that illustrate the pattern of flooding over the entire region.

Chapter 4

Results and Discussion

This chapter is extracted from a paper in review at Journal of Geophysical Research - Oceans.

4.1 Results

We first studied the differences in surge height and timing by using synthetic water level gauges at specific locations within the bay. We divided the bay into three roughly equal (in longitude) sections and chose two water level gauge locations for each section, as shown with the lettered circles in Figure 3.1. Figure 4.1 shows these results. We calculated the mean (solid lines) and median (dashed lines) of each category of simulation for each gauge location. The shaded areas reflect the 5th - 95th percentiles of the simulations in each category.

In all three sections of the bay, the peak surge arrives earlier in the *Location* scenarios than the other scenarios, followed by the *West* scenarios in the west segment of the bay and the

Table 4.1: Peak surge arrival time in minutes from landfall for each synthetic water level gauge in Figure 1 for each category of simulation

	Width	Depth	Width and Depth	Locations	East of Inlet	West of Inlet
Gauge a	94	99	209	13	94	13
Gauge b	60	58	5	15	64	15
Gauge c	42	42	49	28	42	41
Gauge d	41	43	48	29	44	38
Gauge e	85	82	97	35	39	98
Gauge f	93	91	100	42	42	101

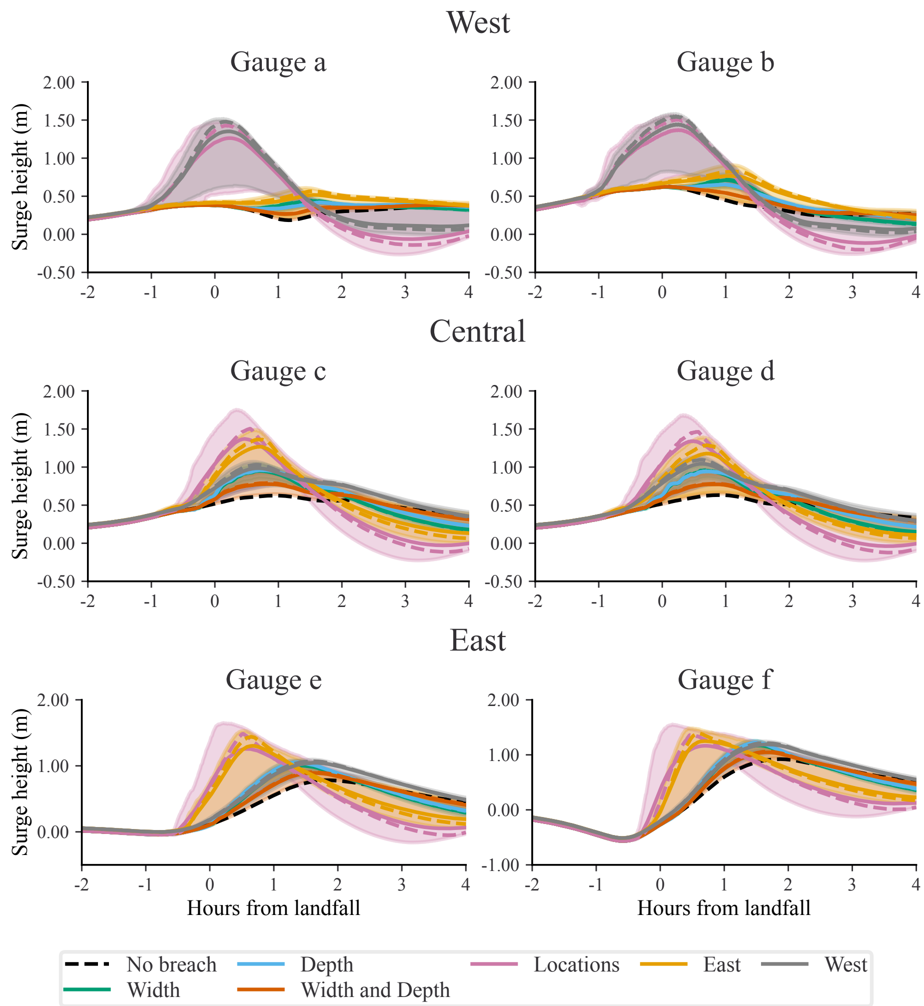

Figure 4.1: Synthetic water level gauges for each section of the bay. See Figure 3.1 for locations. Each dark line is the mean of all of the simulations in that category, the dotted lines in each color represent the median of that category. Each shaded area covers the 5 - 95 percentile of the category

East scenarios in the central and east segments of the bay. The peak surge arrival time for each scenario and gauge is described in Table 4.1. With the exception of the *Width and Depth* scenarios for Gauge b the location surge arrives before the rest of the scenarios. The *Location* surge is also larger for all gauges, as seen in Figure 4.1. The west portion of the bay, the *Location* and *West of Inlet* scenarios are similar in maximum surge. While in the central regions, the maximum surge for the *Location* simulations is larger than the other

Table 4.2: Comparison of L2 norms representing the differences in water level percentiles (5th and 95th) across different gauge locations.

	Width	Depth	Width and Depth	Locations	East of Inlet	West of Inlet
Gauge a	10.07	6.19	15.98	112.30	28.82	91.96
Gauge b	15.89	10.95	23.45	97.89	42.16	79.64
Gauge c	22.03	17.49	34.17	115.71	77.69	33.36
Gauge d	21.47	16.27	32.85	109.37	74.61	37.92
Gauge e	23.54	20.38	34.19	138.75	96.81	29.06
Gauge f	22.77	19.73	33.06	156.11	103.66	28.14

scenarios. Lastly, the maximum surge recorded by the eastern gauges is more consistent across all scenarios. In all cases, the breaching simulations differ from the no breach case.

Table 4.2 is a comparison of the L2 norms for the difference in water levels across different water level gauge locations. We took the difference between the 5th and 95th percentiles for each category of simulation to illustrate the magnitude of the differences in each category of simulation. The variability of the water levels is least in the *Width* and *Depth* simulations for the gauges in the western section of the bay. The *Locations* simulations have the largest variability in the water levels across all gauge locations. The *East of Inlet* and *West of Inlet* water levels exhibit the least variability in the regions opposite to where the breaches occur.

Figure 4.2 illustrates the maximum surge heights for each category of simulation at locations shown as green circles in Figure 3.1. The *Location* simulations have the highest surge with the density peak at 1.85 meters, 1.75 meters, and 1.51 meters for west, central, and east bay respectively.

The standard deviation is also large at 0.32 m, 0.24 m, 0.26 m as compared to the other simulations. When constrained by a maximum of six breaches the *Depth* variations have the largest surge height mean at 1.06 m, 1.07 m, 0.84 m, the median is very similar to the mean for all simulations. The *Width* scenario's mean surge height is 0.97 m, 1.09 m, 0.78 m and the *Width and Depth* simulations have a mean surge height of 0.88 m, 0.98 m, 0.72

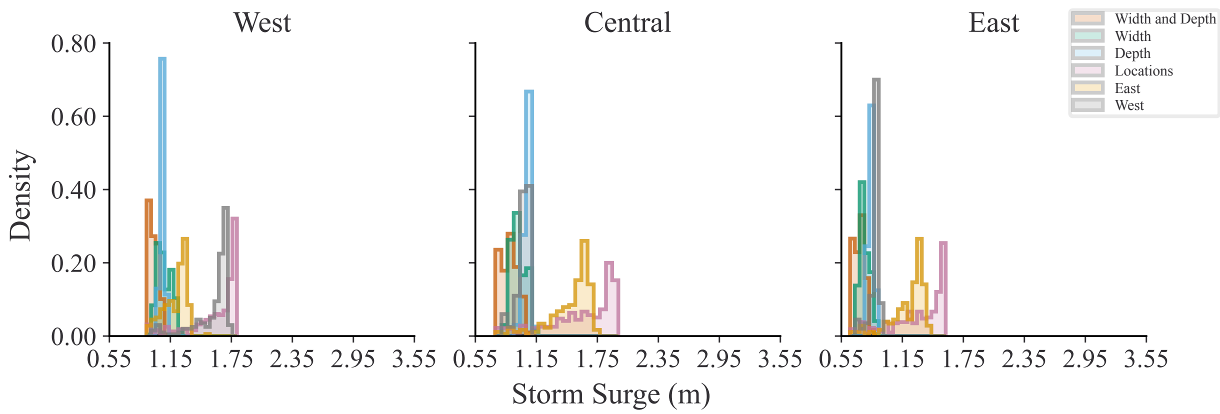

Figure 4.2: Maximum surge height in meters for each selected location shown in Figure 1 (green dots). Data shows 1900 scenarios split into six categories. Six breaches where width is randomized (blue) (464 scenarios), six breaches where depth is randomized (green) (424 scenarios). Varying width, depth, and number of breaches up to six breaches (orange) (297 scenarios). Varying width, depth, location, and number of breaches up to 295 breaches (315). Varying width, depth, number of breaches up to 100 but limiting breach location to the east of the inlet (yellow) (200) and west of the inlet (grey) (west).

m. The *East of Inlet* simulations surge mean is 1.49 m, 1.20 m, 1.21 m, and the mean of the *West of Inlet* simulations is 1.02 m, 1.57 m, 0.88 m. The largest standard deviation of all scenarios varies between the categories if we exclude the *Location*, *East*, and *West* simulations. The largest standard deviation is 0.08 m at the West location for the *Width and Depth*, the Central standard deviation is 0.07 for the *Width* category, and East has a maximum standard deviation of 0.05 m which includes both *Width and Depth* and *Width*. Table 4.3 reports all the results for the surge calculated by GeoClaw.

Figure 4.3 compares the maximum surge for each section of the bay in total. The overall pattern of surge distributions is relatively similar to those at the specific points in the bay in Figure 4.2. The distributions of these data, with the *Location* simulations having the largest impact on surge for each section of the bay. The next largest surge is divided amongst scenarios depending on the bay section, with *West of Inlet* having the largest surge in the west and the *Width* scenarios in the central and east regions.

Table 4.3: Maximum surge height (m) for each category of breach simulations at each of the three points shown on Fig. 4.2

	Width	Depth	Width and Depth	Location	East of Inlet	West of Inlet
west						
Min	0.83	0.79	0.75	0.75	0.79	0.81
Max	1.13	1.12	1.07	1.96	1.73	1.08
Mean	0.97	1.06	0.88	1.60	1.49	1.02
Median	0.96	1.07	0.89	1.69	1.57	1.04
Standard Deviation	0.07	0.04	0.08	0.32	0.21	0.06
Variance	0.00	0.00	0.01	0.10	0.05	0.00
Density Peak	0.94	1.09	0.90	1.85	1.62	1.05
central						
Min	0.95	0.95	0.92	0.92	0.94	0.97
Max	1.25	1.12	1.10	1.80	1.52	1.74
Mean	1.09	1.07	0.98	1.60	1.20	1.57
Median	1.08	1.07	0.98	1.70	1.24	1.66
Standard Deviation	0.07	0.02	0.05	0.24	0.11	0.18
Variance	0.00	0.00	0.00	0.06	0.01	0.03
Density Peak	1.04	1.07	0.93	1.75	1.28	1.67
east						
Min	0.69	0.68	0.64	0.64	0.68	0.70
Max	0.90	0.88	0.84	1.58	1.41	0.93
Mean	0.78	0.84	0.72	1.30	1.21	0.88
Median	0.77	0.85	0.73	1.38	1.28	0.90
Standard Deviation	0.05	0.02	0.05	0.26	0.17	0.05
Variance	0.00	0.00	0.00	0.07	0.03	0.00
Density Peak	0.75	0.86	0.74	1.51	1.31	0.91

Figure 4.4 illustrates the relationship between total cross-sectional breach area (km^2) and total inundation change from a no breach simulation. For all simulations except for *East of Inlet* and *West of Inlet* the relationship shows a logarithmic trend that starts with a minimum inundation of 0.1632 km^2 and illustrates that a larger breach area leads to more inundation to a point, around 75 possible breaches the curve levels off at a total breach area of 0.035 km^2 and an inundation change around 40.1 km^2. Inundation change grows more slowly beyond this point to a maximum total inundation of 49.06 km^2. The second curve from the top is for simulations with the *West of Inlet* scenarios. These simulations still show

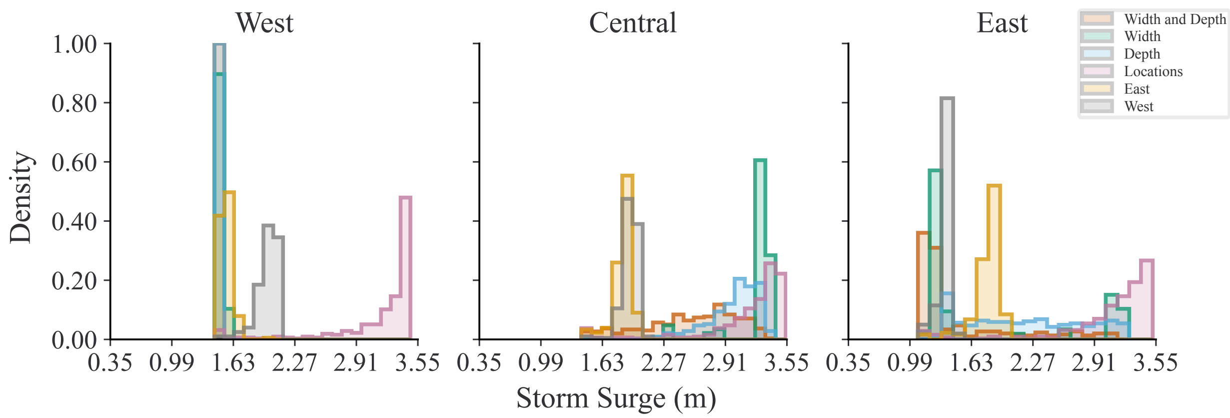

Figure 4.3: Maximum surge height (m) for each category of breach simulations across each entire section of the bay.

a logarithmic trend but level off at a lower total inundation. The third curve is for the *East of Inlet* simulations, which again level off at a lower total inundation.

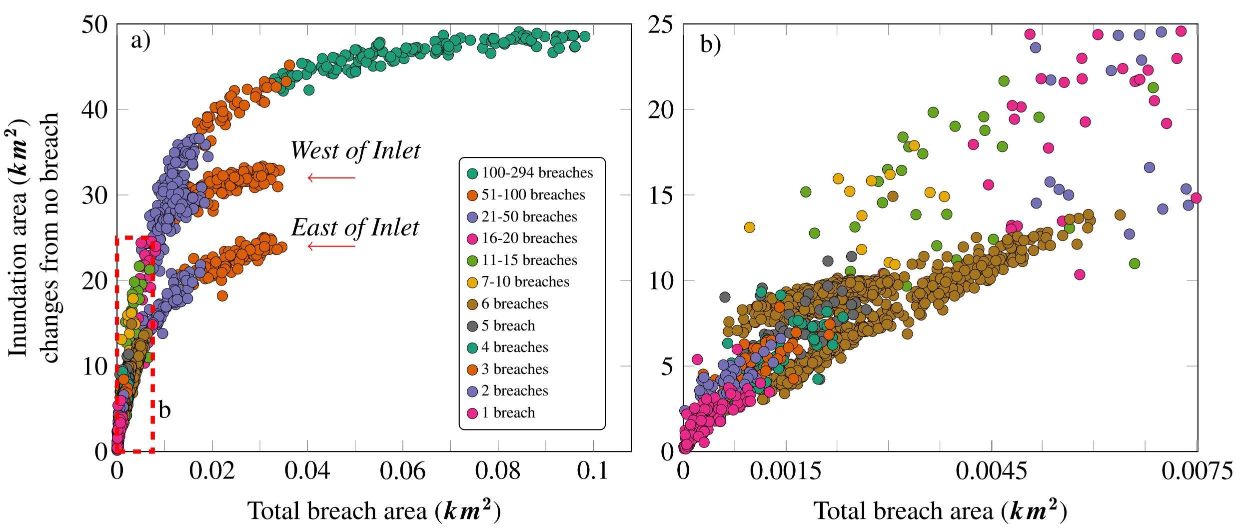

Figure 4.4: a) Total inundation vs. total breach size for all 1900 scenarios, points are colored per number of breaches. b) zoom in of a) panel to show differentiation of breach area and number of breaches and how the inundation can vary

4.2 Discussion

The results of this study illustrate that location, size, and number of breaches have an impact on coastal flooding. There is a clear relationship between total breach area and the amount of flooding in the bay and on the mainland coastline. The histograms plotted in Figure 4.2 illustrate a few different locations within the bay. The west surge point located near the Forge River mouth shows that given the original breaching locations the surge distribution is clustered and overlaps across scenarios, but when the simulations are allowed to vary breach locations the maximum surge is much higher from breaches located nearby. This location has surge pushed initially from the eastern side of the bay and after landfall the surge is pushed again from the western connection to Great South Bay and the nearby breaches. Figures 4.5 and 4.6 further illustrate that the maximum surge in the bay and along the mainland alters due to the location of the breaches. We further discuss the surge patterns of Figures 4.5 and 4.6 below.

The central location is adjacent to the mainland coastline near Seatuck Cove. Varying the breach locations and number of breaches increases the surge, but to a smaller degree than in the west. The maximum surge at the central location is lower than in the west, most likely due to proximity of the inlet. The peak surge that comes from more breaches in the west gets to the inlet before it reaches Seatuck Cove and allows the water to flood out of the bay, reducing the maximum surge for this location. Additionally, the shape of the coastline protects this location to some extent from surge coming from the southwest. However, the surge that comes from the *East of Inlet* breaching is the second-largest surge contributor to this location. Surge that is pushed through the breaches on the east are directed westward by the wind circulation of the hurricane and affect the central location. Figure 4.7a displays the surge patterns from breaching on the eastern section of the island.

The east location, which is closest to the barrier island, has the smallest maximum surge in the bay. Breaches formed eastward of the original locations do bring more surge to this location. However, its proximity to the inlet means that bay surge that travels towards the east after peak ocean surge is past, flows out of the inlet and reduces the total surge possible, and the wind pushes the surge on the eastern side towards the southwest further reducing the total surge possible.

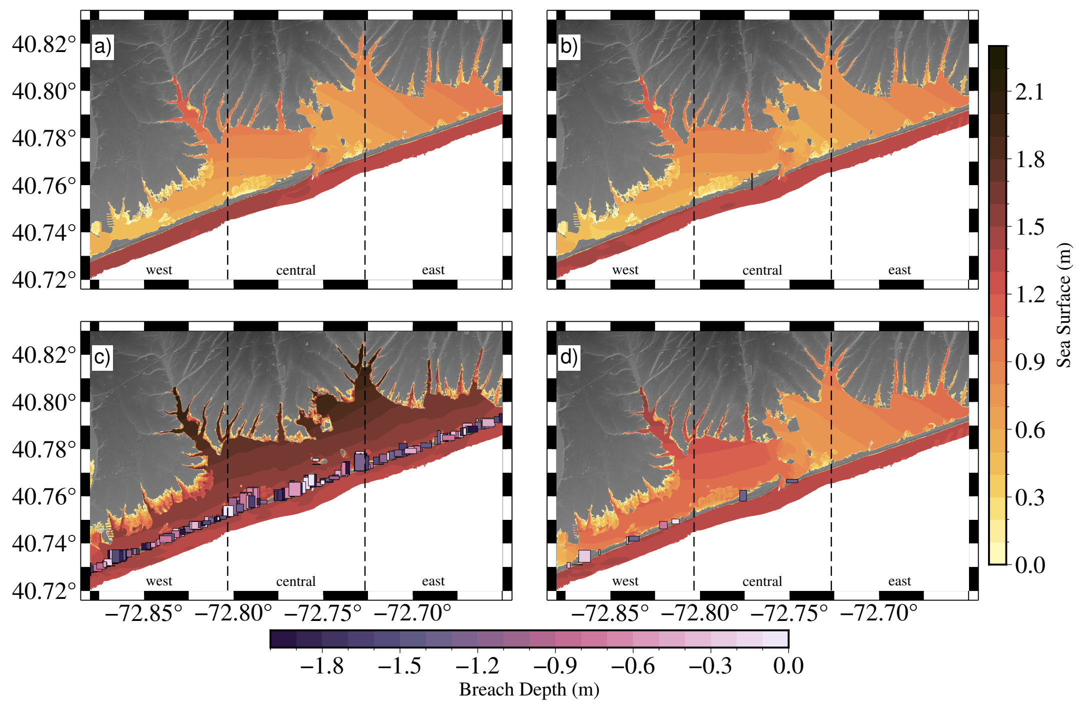

Figure 4.5: Maps Moriches Bay, NY. Each panel is a separate simulation representing different values of storm surge inundation. Panel (a) is our No Breach scenario. Panel (b) is the minimum inundation of 0.162 km^2 with a single small breach. Panel (c) is the largest inundation scenario of 49.06 km^2 with 259 breaches. Panel (d) is a simulation that has the closest inundation to the mean of all 1900 simulations 14.54 km^2, with eleven breaches.

The gauges distributed in each section of the bay display the differences of surge timing and maximum surge amongst the different scenarios as shown in Figure 4.1. Many of the *Location* simulations have breaches in the southwest portion of the barrier island. The peak ocean surge spreads from the southwest towards the northeast before landfall, and the *Location*

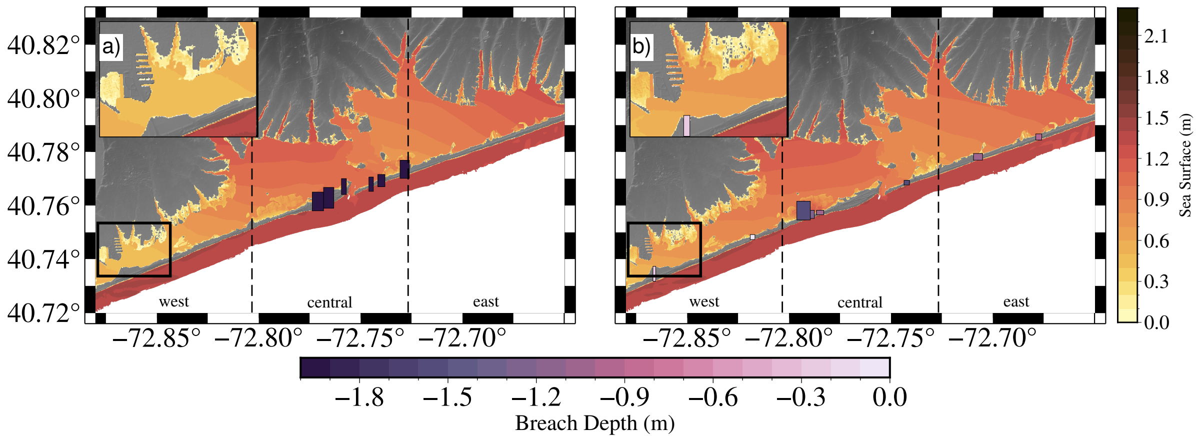

Figure 4.6: a) Maximum surge and inundation for simulations with 6 breaches and total breach area 0.0039 km^2. b) Maximum surge and inundation for simulation that has 11 breaches and a total breach area of 0.0036 km^2.

breaches open earlier than the original breach locations due to this surge timing. This is shown in Figure 4.1 in the west gauges (a and b). The surge arrives earlier and is larger than the other simulations that have breaches closer to the inlet. The central gauges illustrate that while the surge is still larger, the timing is more in sync amongst the *Depth*, *Width*, *Width and Depth*, *East*, *West* scenarios. The eastern gauges maximum surge is not much higher than the other categories of simulations, however the surge does still arrive earlier because of water coming into the bay from breaches in the southwest. Another change that can be seen in Figure 4.1 is in the no breach scenario. Around landfall, the surge is being pushed from the northeast to the southwest. Just after landfall, this direction reverses, and water is pushed in from the connection to Great South Bay. This created a local setdown for a few of the gauges that aren't being protected by the contours of the mainland, gauges a, e, d, in particular show this setdown, which is first seen in gauge a, approximately one hour after landfall and to a smaller extent is seen in gauge c, and gauge d another 30 minutes later. The *Width and Depth* simulations also exhibit this setdown because they affect the bay surge the least amongst all simulations. Once the storm is two to three hours post-landfall, the breaches allow water to flood back out of the bay into the ocean, and we see that with the *Location*, *East of Inlet*, and *West of Inlet* simulations, the water levels at the water level gauges all go down below the no breach scenario, allowing the bay flooding to decrease more rapidly than would be the case if the barrier island was not breached.

Figure 4.4a shows that the total breach dimensions have a relationship to the total area of inundation, with larger and more numerous breaches bringing more water inland. Total breach area across all breaches is the strongest predictor of greater coastal inundation, until the island is significantly eroded, then inundation growth slows considerably. Figure 4.4b brings more nuance to this relationship. While there appears to be a stronger correlation between breach width and inundation, than depth and inundation, breach depth's maximum of two meters is at least a factor of 20 smaller than total width for these scenarios, which reduces the impact depth can have on the hydrodynamics of each breach. The cluster of breaches that hover above the main grouping are the depth scenarios, whereas the width scenarios exhibit a more linear relationship with total inundation area. The secondary and tertiary curves in Figure 4.4a show that inundation is capped if half of the barrier island still exists. These simulations were isolated to only the West and East half of the island on either side of the inlet. Both scenarios have a smaller total impact on inundation, however breaching on the western section of the island contributes to a larger total inundation than the eastern breaches. This is related to the breaching initiating earlier in the west because of the storm's approach direction, also water being pushed out of the inlet as it travels southwest relieves some of the inundation that accumulates on the east.

Figure 4.5 illustrates that different inundation and bay surge patterns are correlated to number and size of breaches. Figure 4.5 panel a) is a no breach scenario which looks very similar in surge and inundation distribution to the minimum inundation (panel b) which has only a single small breach. There are approximately 500 different wet vs. dry cells between these two simulations, which is 163,200 square meters or .1632 square kilometers of inundation. Figure 4.5 panel d) is a simulation that comes closest to the mean of all the inundation change from all 1900 simulations. There are eleven medium-sized breaches with a total breach area of .0029 km^2 and total inundation change of 14.54 km^2. The simulation that comes closest to the median of the scenarios (not pictured) has six medium-sized breaches, with a total inundation of 9.36 km^2. The shape of the contours of surge in the bay and the total horizontal coastal inundation is very different from the no breach or minimum inundation scenarios, with higher flooding potential in the coves, creeks and rivers that border the bay and along the lower elevation coastlines. Lastly the maximum inundation scenario is one where most of the island has been breached, this scenario has a bay surge of approximately two meters in most areas and the lowest elevation areas of the coastline are completely flooded.

The impact differing breach locations has on inundation, as illustrated in Figure 4.5c, can be further seen in Figure 4.6. This figure shows the differences between two simulations with a similar total breach area; however, the total inundation is very different. Figure 4.6a, shows a scenario with six moderately sized breaches in the locations that occurred during the 1938 hurricane, the total breach area is .0039 km^2, and total inundation is 10.44 km^2. Figure 4.6b, has a smaller total breach area of .0036 km^2 but a larger inundation at 12.03 km^2. The breaches in this scenario are generally smaller but more spaced out across the barrier island, with several in the western portion of the barrier island closer to Great South Bay. While the pattern of surge in the bay is similar, the contours of the bay surge differ, and the breaches in the connection between Great South Bay and Moriches Bay allow more water to flow in from the southwest prior to peak ocean surge. This creates more coastal inundation along the western coastline, see inset of Figures 4.6a and b. The Forge River surge is higher in Figure 4.6b and the inlet region has a lower total water depth. The eastern portion of the bay has less inundation in 4.6b, most likely due to the majority of the breaches being towards the west, plus the inlet allowing water to flow out of the bay, and the elevation along the coastline is lower on the western half of the bay.

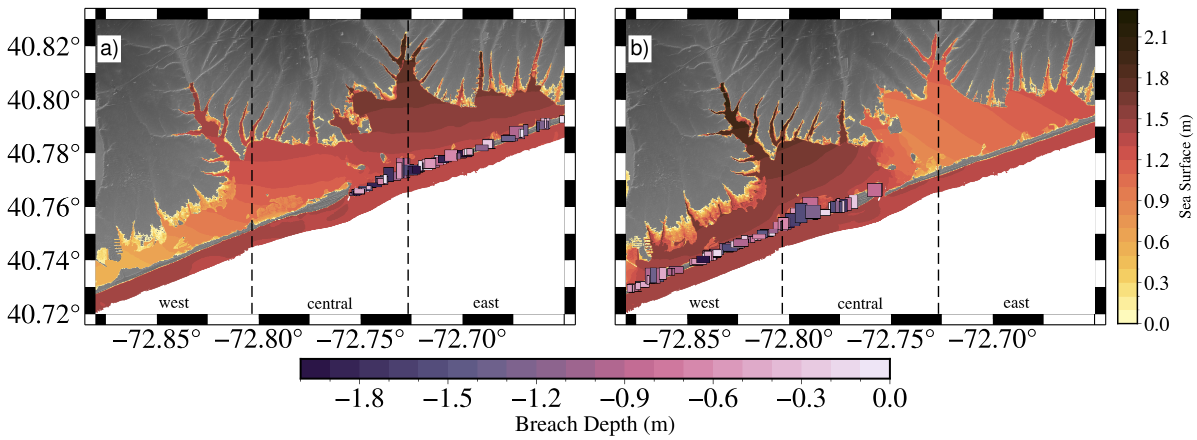

Figure 4.7: a) Maximum surge and inundation for *East of Inlet* simulations with a total inundation of 24.87 km^2. b) Maximum surge and inundation for *West of Inlet* simulation that has a total breach area of 26.85 km^2.

Breaching isolated to one side of the inlet or the other also creates interesting changes in the bay surge and total inundation. Figure 4.7 highlights some of these changes. As Figure 4.4 shows, the *West of Inlet* scenarios produce a higher total coastal inundation which is further seen in Figure 4.7b where the western mainland coastline is significantly inundated as compared to other scenarios. However, the *East of Inlet* simulations have the ability to push the surge further down the bay due to the direction of the wind forcing and as the storm continues past landfall not all of the surge floods out of the inlet.

Figures 4.5, 4.6, and 4.7 highlight the important details across the different simulations. Total breach area is a very strong predictor of total inundation. However, location of breaching is also very important, especially given the dynamics of the storm forcing and direction with which the surge is being pushed. While this study does not include tides and waves, they do play an important role in the dynamics of the surge in the bay and, further, are a strong contributor to breach initiation and growth. However, there is a stochastic nature to these processes that is difficult to model and much of our understanding comes from empirical observations. Adding a tidal or wave component to our simulations could result in different patterns of breaching and inundation. Our use of breaching based on offshore water levels allows us to assume that wave action has contributed to breach initiation based on previous studies and observations on how breaches form.

Chapter 5

Conclusions

5.1 Summary

This dissertation has presented the role that barrier island breach has on the impacts of mainland inundation and bay surge distributions for a barrier island system near Moriches, NY. Chapter 3 described the model changes and additions that we needed to be able to run many hundreds of simulations to gain a statistical understanding of the impacts of breaching. A straightforward reduction on dune height over a barrier island at specific locations eliminated the complexity of the nature of how breaches form and isolated solely the flooding and inundation changes to the mainland and back-barrier bay. Broadening the capability of GeoClaw to enable the use of PBL model wind and pressure fields allowed myself and others to use GeoClaw for storm surge modeling with additional storm inputs. The many types of simulations allowed for the exploration of how different numbers of breaches, their locations, and sizes change the total inundation along the mainland coastline. Chapter 4 illustrated the results of my 1900 simulations and how those results can be interpreted.

5.2 Conclusions

Breaching of a barrier island during a hurricane shows a strong impact on mainland inundation. The number, locations, and size of the breaches can change the inundation potential for the coastline. Breaching location has the most impact on total inundation and can also change the timing of the maximum surge, depending on the location of the breaches and how the storm approaches the region of interest. Breach width has a stronger impact than breach depth, but most likely due to the width being a factor of 20 larger than the total depth. These characteristics can aid in our understanding of what are the most vulnerable areas in a barrier island and how breaching impacts them, and can provide opportunities for shoring up infrastructure and allowing planning that minimizes the storm's disruption to lives and the community.

5.3 Future Work

This study was limited in its extent due to the location and orientation of the barrier island we studied. A single storm approaching the region for a direct hit close to the barrier island leads to further limitations on the impacts that can be extrapolated from my results. Future work can include:

- Run many more simulations, so there are thousands of results for each category to gain a better agreement on the statistics of the inundation changes.
- Update the breaching algorithm so that is shore perpendicular, instead of simply north-south, to better match the orientation of the barrier island.
- Using the same study parameters, vary the storms being modeled to include larger, smaller, and storms with a slower forward speed.
- Varying the approach of the hurricanes to include bypassing and direct hits but in different locations.

- Running additional studies to include other barrier island systems, that would include different orientations of the coastline.

Adding these different study variables can aid in our understanding of how breaching impacts all regions and communities around the US and the world, and would provide a better understanding of coastal vulnerabilities and how these regions can best be planned to reduce the risks.

Bibliography

[1] Paul D. Bates, Niall Quinn, Christopher Sampson, Andrew Smith, Oliver Wing, Jeison Sosa, James Savage, Gaia Olcese, Jeff Neal, Guy Schumann, Laura Giustarini, Gemma Coxon, Jeremy R. Porter, Mike F. Amodeo, Ziyan Chu, Sharai Lewis-Gruss, Neil B. Freeman, Trevor Houser, Michael Delgado, Ali Hamidi, Ian Bolliger, Kelly E. McCusker, Kerry Emanuel, Celso M. Ferreira, Arslaan Khalid, Ivan D. Haigh, Anaïs Couasnon, Robert E. Kopp, Solomon Hsiang, and Witold F. Krajewski. Combined modeling of us fluvial, pluvial, and coastal flood hazard under current and future climates. *Water Resources Research*, 57(2):e2020WR028673, 2021. doi: https://doi.org/10.1029/2020WR028673. URL https://onlinelibrary.wiley.com/doi/abs/10.1029/2020WR028673. e2020WR028673 2020WR028673.

[2] Marsha J. Berger, David L. George, Randall J. LeVeque, and Kyle T. Mandli. The GeoClaw software for depth-averaged flows with adaptive refinement. *Advances in Water Resources*, 34(9):1195–1206, 9 2011. ISSN 03091708. doi: 10.1016/j.advwatres.2011.02.016. URL http://linkinghub.elsevier.com/retrieve/pii/S0309170811000480.

[3] Marsha J Berger, David L George, Randall J LeVeque, and Kyle T Mandli. The geoclaw software for depth-averaged flows with adaptive refinement. *Advances in Water Resources*, 34(9):1195–1206, 2011.

[4] Cheryl A Blain, Robert S Linzell, Philip Chu, and Chris Massey. Validation test report for the advanced circulation model (adcirc) v45. 11. *NRL Memorandum Report, NRL/MR/7320–10-9205, Naval Research Laboratory2010*, 2010.

[5] Eric S. Blake, Tpc Miami, Edward N. Rappaport, Jerry D. Jarrell, and Christopher W.

Landsea. The deadliest, costliest, and most intense united states tropical cyclones from 1851 to 2004 (and other frequently requested hurricane facts). Technical report, National Oceanographic and Atmospheric Administration, 2005. URL https://api.semanticscholar.org/CorpusID:131697406.

[6] I V Buynevich. Geological signatures of barrier breaching and overwash. *Journal of Coastal Research*, 2004(39):112–116, 2006. ISSN <null>.

[7] IV Buynevich and JP Donnelly. Geological signatures of barrier breaching and overwash, southern massachusetts, usa. *Journal of Coastal Research*, pages 112–116, 2006.

[8] Rafael Cañizares and Jennifer L. Irish. Simulation of storm-induced barrier island morphodynamics and flooding. *Coastal Engineering*, 55(12):1089–1101, 2008. ISSN 03783839. doi: 10.1016/j.coastaleng.2008.04.006. URL http://dx.doi.org/10.1016/j.coastaleng.2008.04.006.

[9] Center for Operational Oceanographic Products and Services (CO-OPS). CO-OPS 1-minute Tsunami Water Level Data. NOAA National Centers for Environmental Information, 2007. [April 5, 2021].

[10] Mary A Cialone, T Chris Massey, Mary E Anderson, Alison S Grzegorzewski, Robert E Jensen, Alan Cialone, David J Mark, Kimberly C Pevey, Brittany L Gunkel, and Tate O McAlpin. North atlantic coast comprehensive study (naccs) coastal storm model simulations: Waves and water levels. Technical report, Engineer Research and Development Center, 2015.

[11] Mary A. Cialone, Alison S. Grzegorzewski, David J. Mark, Mary A. Bryant, and Thomas C. Massey. Coastal-storm model development and water-level validation for the north atlantic coast comprehensive study. *Journal of Waterway, Port,*

Coastal, and Ocean Engineering, 143(5):04017031, 2017. doi: 10.1061/(ASCE)WW.1943-5460.0000408. URL https://ascelibrary.org/doi/abs/10.1061/%28ASCE%29WW.1943-5460.0000408.

[12] Clawpack Development Team. Clawpack software, 2020. URL http://www.clawpack.org. Version 5.9.2.

[13] Nicholas K Coch. Hurricane hazards along the northeastern atlantic coast of the united states. *Journal of Coastal Research*, pages 115–147, 1994.

[14] WC Conner, Raymond H Kraft, and D Lee Harris. Empirical methods for forecasting the maximum storm tide due to hurricanes and other tropical storms. *Monthly Weather Review*, 85(4):113–116, 1957.

[15] Andrea Conver, Julie Sepanik, Bobby Louangsaysongkham, and S Miller. Sea, lake, and overland surges from hurricanes (slosh) basin development handbook v2. 0. *Silver Springs, MD: NOAA/NWS/Meteorological Development Laboratory*, 2008.

[16] Cooperative Institute for Research in Environmental Sciences. Continuously updated digital elevation model (CUDEM) - 1/9 arc-second resolution bathymetric-topographic tiles, 2021.

[17] Harry de Loof, Henk J. Steetzel, Arie W. Kraak, Harry de Looff, Henk J. Steetzel, Arie W. Kraak, Harry de Loof, Henk J. Steetzel, and Arie W. Kraak. Breach growth: Experiments and modelling. *Coastal Engineering 1996*, pages 2746–2755, 1997. ISSN 0369-4194. doi: 10.2473/shigentosozai1953.80.915{_}833.

[18] Jason G. Fleming, Crystal W. Fulcher, Richard A. Luettich, Brett D. Estrade, Gabrielle D. Allen, and Harley S. Winer. *A Real Time Storm Surge Forecasting Sys-*

tem Using ADCIRC, pages 893–912. ASCE, 2007. doi: 10.1061/40990(324)48. URL https://ascelibrary.org/doi/abs/10.1061/40990%28324%2948.

[19] Ashley Elizabeth Frey. *The Impact of Climate Change on Hurricane Flooding Inundation, Property Damages, and Population Affected*. PhD thesis, Texas A & M University, 2008.

[20] Bob Glahn, Arthur Taylor, Nicole Kurkowski, and Wilson A Shaffer. The role of the slosh model in national weather service storm surge forecasting. *National Weather Digest*, 33(1):3–14, 2009.

[21] Frank I González, Randall J LeVeque, Paul Chamberlain, Bryant Hirai, Jonathan Varkovitzky, and David L George. Validation of the geoclaw model. In *NTHMP MMS Tsunami Inundation Model Validation Workshop. GeoClaw Tsunami Modeling Group*, 2011.

[22] D. Lee Harris. The hurricane surge. *Coastal Engineering Proceedings*, 1(6):5, Jan. 1957. doi: 10.9753/icce.v6.5. URL https://icce-ojs-tamu.tdl.org/icce/article/view/1870.

[23] Craig Harter and Jens Figlus. Numerical modeling of the morphodynamic response of a low-lying barrier island beach and foredune system inundated during Hurricane Ike using XBeach and CSHORE. *Coastal Engineering*, 120(April 2016):64–74, 2017. ISSN 03783839. doi: 10.1016/j.coastaleng.2016.11.005. URL http://dx.doi.org/10.1016/j.coastaleng.2016.11.005.

[24] Steven WH Hoagland, Catherine R Jeffries, Jennifer L Irish, Robert Weiss, Kyle Mandli, Sean Vitousek, Catherine M Johnson, and Mary A Cialone. Advances in morphodynamic modeling of coastal barriers: a review. *Journal of Waterway, Port, Coastal, and Ocean Engineering*, 149(5):03123001, 2023.

[25] Greg J. Holland. An analytic model of the wind and pressure profiles in hurricanes. *Monthly Weather Review*, 108(8):1212 – 1218, 1980. doi: 10.1175/1520-0493(1980)108<1212:AAMOTW>2.0.CO;2. URL https://journals.ametsoc.org/view/journals/mwre/108/8/1520-0493_1980_108_1212_aamotw_2_0_co_2.xml.

[26] Robert A Hoover. Empirical relationships of the central pressures in hurricanes to the maximum surge and storm tide. *Monthly Weather Review*, 85(5):167–174, 1957.

[27] Jennifer L Irish, Ashley E Frey, Julie D Rosati, Francisco Olivera, Lauren M Dunkin, James M Kaihatu, Celso M Ferreira, and Billy L Edge. Potential implications of global warming and barrier island degradation on future hurricane inundation, property damages, and population impacted. *Ocean & Coastal Management*, 53(10):645–657, 2010.

[28] Catherine R Jeffries and Kyle Mandli. Adapting data derived storm products for use in geoclaw. https://github.com/cjeffr/geoclaw/tree/OWI_integration, 2022.

[29] Chester P Jelesnianski. Splash:(special program to list amplitudes of surges from hurricanes). i, landfall storms. Technical report, National Oceanographic and Atmospheric Admininstration; National Weather Service, 1972.

[30] Chester P Jelesnianski. *A preliminary view of storm surges before and after storm modifications*, volume 3. Environmental Research Laboratories, Weather Modification Program Office, 1973.

[31] Chester P Jelesnianski. *SLOSH: Sea, lake, and overland surges from hurricanes*, volume 48. US Department of Commerce, National Oceanic and Atmospheric Administration ..., 1992.

[32] Bradley D Johnson, Nobuhisa Kobayashi, and Mark B Gravens. Cross-Shore Numerical Model CSHORE for Waves , Currents , Sediment Transport and Beach Profile Evolution

Coastal and Hydraulics Laboratory Cross-Shore Numerical Model CSHORE for Waves , Currents , Sediment Transport and Beach. Technical Report September, US Army Corps of Engineers, 2012.

[33] Nicholas C Kraus. Analytical model of incipient breaching of coastal barriers. *Coastal Engineering Journal*, 45(04):511–531, 2003.

[34] NICHOLAS C. KRAUS and KENTARO HAYASHI. *NUMERICAL MORPHOLOGIC MODEL OF BARRIER ISLAND BREACHING*, pages 2120–2132. Coastal Engineering, 2005. doi: 10.1142/9789812701916_0170. URL https://www.worldscientific.com/doi/abs/10.1142/9789812701916_0170.

[35] Nicholas C Kraus and Ty V Wamsley. Coastal Barrier Breaching , Part 1 : Overview of Breaching Processes. Technical Report March, US Army Corps of Engineers, 2003.

[36] Nicholas C Kraus, Adele Militello, and Gary Todoroff. Barrier Breaching Processes and Barrier Spit Breach, Stone Lagoon, California. *Shore & Beach*, 70(4), 2002. ISSN 00045772.

[37] Nicholas C Kraus, Adele Militello, and Gary Todoroff. Barrier breaching processes and barrier spit breach, stone lagoon, california. *Shore & Beach*, 70(4):21–28, 2002.

[38] Christopher W. Landsea and James L. Franklin. Atlantic hurricane database uncertainty and presentation of a new database format. *Monthly Weather Review*, 141(10):3576 – 3592, 2013. doi: 10.1175/MWR-D-12-00254.1. URL https://doi.org/10.1175/MWR-D-12-00254.1.

[39] Stephen P Leatherman. Beach erosion, tidal inlets and politics: The fire island story. *Shore & Beach*, 67, 1999.

[40] Randall J LeVeque. Clawpack: A software package for solving multi-dimensional conservation laws. In *Proc. 5th Intl. Conf. Hyperbolic Problems*, pages 188–197. Citeseer, 1994.

[41] Kyle T Mandli and Clint N Dawson. Adaptive mesh refinement for storm surge. *Ocean Modelling*, 75:36–50, 2014.

[42] Kyle T Mandli, Aron J Ahmadia, Marsha Berger, Donna Calhoun, David L George, Yiannis Hadjimichael, David I Ketcheson, Grady I Lemoine, and Randall J LeVeque. Clawpack: building an open source ecosystem for solving hyperbolic pdes. *PeerJ Computer Science*, 2:e68, 2016.

[43] Gordon McGranahan, Deborah Balk, and Bridget Anderson. The rising tide: assessing the risks of climate change and human settlements in low elevation coastal zones. *Environment and Urbanization*, 19(1):17–37, 2007. doi: 10.1177/0956247807076960. URL https://doi.org/10.1177/0956247807076960.

[44] Andrew Morang. *Shinnecock Inlet, New York, Site Investigation, Report 1: Morphology and Historical Behaviour*. US Army Corps of Engineers Waterways Experiment Station, 1999.

[45] Norberto C Nadal-Caraballo, Jeffrey A Melby, Victor M Gonzalez, and Andrew T Cox. Coastal storm hazards from virginia to maine. Technical report, US Army Corps of Engineers, 2015. URL https://hdl.handle.net/11681/7715.

[46] National Hurricane Center. Hurricane Preparedness - Hazards, 2006. URL https://www.nhc.noaa.gov/prepare/hazards.php.

[47] Barbara Neumann, Athanasios T. Vafeidis, Juliane Zimmermann, and Robert J. Nicholls. Future coastal population growth and exposure to sea-level rise and coastal

flooding - a global assessment. *PLOS ONE*, 10(3):1–34, 03 2015. doi: 10.1371/journal.pone.0118571. URL https://doi.org/10.1371/journal.pone.0118571.

[48] George F Oertel. The barrier island system, 1985.

[49] J.W. Pierce. Tidal Inlets and Washover Fans Author. *The Journal of Geology*, 78(2): 230–234, 1970. URL http://www.jstor.org/stable/30063791.

[50] JW Pierce. Tidal inlets and washover fans. *The Journal of Geology*, 78(2):230–234, 1970.

[51] Dano Roelvink, Ad Reniers, AP Van Dongeren, Jaap Van Thiel De Vries, Robert McCall, and Jamie Lescinski. Modelling storm impacts on beaches, dunes and barrier islands. *Coastal engineering*, 56(11-12):1133–1152, 2009.

[52] Dano Roelvink, Ad Reniers, Ap Van Dongeren, Jaap Van Thiel De Vries, Jamie Lescinski, and Robert McCall. Modeling storm impacts on beaches, dunes and barrier islands. *Proceedings of the Coastal Engineering Conference*, 56(11-12):1684–1696, 2009. ISSN 01613782. doi: 10.1016/j.coastaleng.2009.08.006. URL http://dx.doi.org/10.1016/j.coastaleng.2009.08.006.

[53] Jr. Sallenger A.H. Storm impact scale for barrier islands. *Journal of Coastal Research*, 16(3):890–895, 2000.

[54] E. J. Schmeltz, R. M. Sorensen, M. J. McCarthy, and G. Nersesian. Breach/Inlet Interaction At Moriches Inlet. *Proceedings of the Coastal Engineering Conference*, 2: 1062–1077, 1983. ISSN 0589-087X. doi: 10.9753/icce.v18.66.

[55] E.J. Schmeltz, R.M. Sorensen, M.J. McCarthy, and G. Nersesian. *Breach/Inlet Interaction at Moriches Inlet*, pages 1062–1077. Coastal Engineering, 1982.

doi: 10.1061/9780872623736.066. URL https://ascelibrary.org/doi/abs/10.1061/9780872623736.066.

[56] Christopher R Sherwood, Joseph W Long, Patrick J Dickhudt, P Soupy Dalyander, David M Thompson, and Nathaniel G Plant. Inundation of a barrier island (Chandeleur Islands, Louisiana, USA) during a hurricane: Observed water-level gradients and modeled seaward sand transport. *Journal of Geophysical Research: Earth Surface*, 119 (7):1–18, 2014. ISSN 2169-9003. doi: 10.1002/2013JF003069.Received.

[57] Stephanie M. Smallegan and Jennifer L. Irish. Barrier island morphological change by bay-side storm surge. *Journal of Waterway, Port, Coastal and Ocean Engineering*, 143 (5):1–10, 2017. ISSN 0733950X. doi: 10.1061/(ASCE)WW.1943-5460.0000413.

[58] Stephanie M Smallegan and Jennifer L Irish. Barrier island morphological change by bay-side storm surge. *Journal of Waterway, Port, Coastal, and Ocean Engineering*, 143 (5):04017025, 2017.

[59] Matthew L Stutz and Orrin H Pilkey. A review of global barrier island distribution. *Journal of Coastal Research*, pages 15–22, 2001.

[60] Elizabeth Valenti and Patrick Fitzpatrick. Forecasting of storm-surge floods using adcirc and optimized dems. Technical report, NASA, 2006.

[61] Marlies A. van der Lugt, Ellen Quataert, Ap van Dongeren, Maarten van Ormondt, and Christopher R. Sherwood. Morphodynamic modeling of the response of two barrier islands to Atlantic hurricane forcing. *Estuarine, Coastal and Shelf Science*, 229(May): 106404, 2019. ISSN 02727714. doi: 10.1016/j.ecss.2019.106404. URL https://doi.org/10.1016/j.ecss.2019.106404.

[62] Marlies A van der Lugt, Ellen Quataert, Ap van Dongeren, Maarten van Ormondt,

and Christopher R Sherwood. Morphodynamic modeling of the response of two barrier islands to atlantic hurricane forcing. *Estuarine, Coastal and Shelf Science*, 229:106404, 2019.

[63] Paul J. Visser. A model for breach erosion in sand-dikes. *Coastal Engineering 2000 - Proceedings of the 27th International Conference on Coastal Engineering, ICCE 2000*, 276:3829–3842, 1994. doi: 10.1061/9780784404119.267.

[64] Paul J Visser. Breach erosion in sand-dikes. In *Coastal Engineering 1998*, pages 3516–3528. Coastal Engineering, 1999.

[65] Paul J Visser. Breach erosion in sand-dikes. In *Coastal Engineering 1998*, pages 3516–3528. Coastal Engineering, 1999.

[66] Ty V Wamsley and Nicholas C Kraus. Coastal Barrier Island Breaching, Part 2: Mechanical Breaching and Breach Closure. Technical Report August, US Army Corps of Engineers, 2005.

[67] Ty V Wamsley and Nicholas C Kraus. Coastal barrier island breaching, part 2: Mechanical breaching and breach closure. *Coastal and Hydraulic Laboratory Technical Note ERDC/CHL CHETN IV-65, US Army Engineer Research and Development Center, Vicksburg, MS*, 21, 2005.

[68] Pauline Weatherall, Karen M Marks, Martin Jakobsson, Thierry Schmitt, Shin Tani, Jan Erik Arndt, Marzia Rovere, Dale Chayes, Vicki Ferrini, and Rochelle Wigley. A new digital bathymetric model of the world's oceans. *Earth and space Science*, 2(8): 331–345, 2015.

[69] Joannes J Westerink, Richard A Luettich, Jesse C Feyen, John H Atkinson, Clint Dawson, Hugh J Roberts, Mark D Powell, Jason P Dunion, Ethan J Kubatko, and Hasan

Pourtaheri. A basin-to channel-scale unstructured grid hurricane storm surge model applied to southern louisiana. *Monthly weather review*, 136(3):833–864, 2008.

[70] Keqi Zhang and Stephen Leatherman. Barrier island population along the us atlantic and gulf coasts. *Journal of Coastal Research*, 27(2):356–363, 2011.